Received: 21 November 2023 | Revised: 5 January 2024 | Accepted: 8 January 2024

DOI: 10.1002/pol.20230876

RESEARCH ARTICLE

JOURNAL OF POLYMER SCIENCE WILEY

Application of artificial neural network to evaluation of dimensional accuracy of 3D-printed polylactic acid parts

Seyhmus Gunes[1] | **Osman Ulkir**[2] | **Melih Kuncan**[3]

[1]Department of Energy Systems, Mus Alparslan University, Mus, Turkey

[2]Department of Electric and Energy, Mus Alparslan University, Mus, Turkey

[3]Department of Electrical and Electronics Engineering, Siirt University, Siirt, Turkey

Correspondence
Osman Ulkir, Department of Electric and Energy, Mus Alparslan University, Mus 49210, Turkey.
Email: o.ulkir@alparslan.edu.tr

Abstract

Additive manufacturing (AM) has begun to replace traditional fabrication because of its advantages, such as easy manufacturing of parts with complex geometry, and mass production. The most important limitation of AM is that dimensional accuracy cannot be achieved in all parts. Dimensional accuracy is essential for high reliability, high performance, and useful final products. This study investigates the impact of printing parameters on the dimensional accuracy of samples fabricated through fused deposition modeling (FDM), an additive manufacturing (AM) method utilizing polylactic acid (PLA) material. The experimental design process was performed using Taguchi methodology. ANOVA was used to determine the most important parameter affecting accuracy. Based on experimental studies, the optimal printing parameters for parts are determined as follows: concentric infill pattern, 3 mm wall thickness, 70% infill density, and a layer thickness of 200 μm. Artificial neural network (ANN) was used in the evaluation and prediction of the results. The *R*-square (R^2) performance evaluation criterion was above 95% from the ANN results. This value shows that the results are significant. The data acquired from this study may assist in identifying optimal parameters that contribute to the fabrication of samples with high dimensional accuracy using the FDM method.

KEYWORDS

3D printing, additive manufacturing, ANOVA, artificial neural network, dimensional accuracy, polylactic acid, Taguchi method

1 | INTRODUCTION

Additive manufacturing (AM) or 3D printing method is the process of manufacturing material in layers to obtain a final product. Rapid prototyping of models developed in 3D with computer-aided design (CAD) software is possible with this method.[1,2] AM technology has begun to replace traditional fabrication methods because of its advantages, such as design flexibility, production of complex geometric structures, efficient material consumption, and low device cost.[3] Nowadays, it is possible to see 3D printed products in many fields, such as healthcare, architecture, agriculture, robotics, drones, space, and automotive.[4–8]

There are many AM methods available depending on the type of material used.[9,10] In this study, polylactic acid (PLA), which is a polymer-based thermoplastic, was used. A fused deposition modeling (FDM) based 3D printer device was employed for fabrication. Thermoplastics used

in FDM other than PLA material are as follows[11–15]: acrylonitrile butadiene styrene (ABS), thermoplastic polyurethane (TPU), polyethylene terephthalate glycol (PETG), and wood. FDM is one of the most preferred AM methods because of its ease of use, wide range of materials, and low device cost.[16,17] The FDM process begins by melting a filament or plastic wire in a thermal print head. This head follows a specific pattern and thus applies the melted plastic material layer by layer onto the surface.[18] These layers stick together and harden after cooling. As a result, the final product takes its final shape.[19,20] The printing parameters chosen during the FDM fabrication process are essential as they affect the mechanical properties, quality, and dimensional accuracy of the product.[21–23] In this process, there are many printing parameters, such as layer thickness, nozzle temperature, table temperature, wall thickness, raster angle, and printing speed.[24–26] The parameter selection should be made according to which feature of the product is desired to be investigated. This feature may be due to factors, such as surface roughness, dimensional accuracy, energy consumption, and tensile strength.[27–30] In this study, four printing parameters (infill pattern, wall thickness, infill density, and layer thickness) that have a high impact on dimensional accuracy were selected because of the studies examined. These parameters have not been examined in any study in terms of the dimensional accuracy of additively manufactured parts.

The 3D printing process has many manufacturing limitations, such as low mechanical strength, poor surface quality, and low-dimensional accuracy.[31–33] Experimental design rules can be used to identify these limitations and dimensional accuracy. The dimensional accuracy of the final products can be observed using different printing parameters in AM throughout the design process. The design and fabrication of a proposed test model depends on many parameters, such as the nozzle diameter and resolution of the 3D printer used.[34–36] There is a geometric limitation to the small parts that 3D printers can produce. The concept of dimensional accuracy is a critical feature for product quality at the desired level in many fabrication technologies. The outcome of this study is to obtain the least dimensional deviation. The 3D printer and printing parameters used in the AM fabrication phase directly affect the measurement accuracy. Thus, researchers are working to determine the optimum printing parameters and manufacturing devices required for the high dimensional accuracy of 3D printed parts.[37,38] Recently developed machine learning (ML) algorithms have begun to be used in manufacturing technologies to optimize and predict the AM process.[39–42] However, there are limited studies for ML on the dimensional accuracy of parts. This study examined the dimensional accuracy of parts with different geometric structures using an artificial neural network (ANN) method. This method is one of the ML strategies used to improve the model's fit and the accuracy of the correlation between anticipated and experimental results.[43] ANNs have become one of the most popular ML approaches because of their ability to model nonlinear data and extract complex relationships between input and output parameters. ANNs are well-known in the field of material science for their capacity to explore the nonlinear behavior of materials.[44] ANNs have been employed for modeling and optimization in a variety of materials because of their flexible working and capacity to understand any type of problem.[45,46]

There are limited studies in the literature regarding the dimensional accuracy of 3D products fabricated using the FDM technique and the effect of printing parameters on this.[47,48] Hanon et al. examined the effect of printing parameters on the dimensional accuracy of samples produced with PLA material.[49] Cylindrical and dog-bone tensile test samples were produced using different printing parameters based on FDM, including build orientation, raster direction angle, and layer thickness. The layer thickness has a very high effect on accuracy among the parameters. According to the results, a high dimensional accuracy (98.829%) was achieved for the samples. Akbas et al. experimentally and numerically analyzed the effect of nozzle temperature and feed rates on the dimensions of FDM polymer parts.[50] A linear regression model was built on the basis of experimental data to understand the correlation between printing parameters. The results showed that the numerical model predictions were in good agreement with the experimental data. Bayraklilar worked on determining the optimum parameters required to improve the dimensional accuracy of the AM method.[51] Optimum parameters were determined for the dimensional accuracy of samples fabricated with FDM using ABS material. ANN was used to predict the experimental results. Mohamed et al. investigated the effects of FDM manufacturing conditions on the dimensional accuracy of cylindrical parts.[52] In this study, a new class of experimental design techniques is proposed for integrated second-order descriptive scan design (DSD) and ANN to design experiments to evaluate and predict printing parameters. The results show that a DSD integrated with an ANN is a more attractive and promising technique for AM applications. Ekinci and Ehrmann examined the dimensional accuracy of FDM printed objects with sharp inner or outer corners depending on the printing parameters.[53] The results showed that different adhesion aids lead to a change in the dimensional accuracy, which can be used to optimize this parameter.

The dimensional accuracy of 3D printed samples is generally examined based on a uniform shape. In this study, the effect of printing parameters on the dimensional accuracy of 3D-printed cylindrical, triangular, and pentagonal samples was determined. The effect of printing parameters on material consumption and printing time was also examined besides the accuracy. The samples were

fabricated on an FDM 3D printer using PLA material. The experimental design process was performed using Taguchi methodology. The Taguchi L9 orthogonal array was employed with the following design parameters: infill pattern, wall thickness, infill density, and layer thickness. Experimental studies determined by this method were conducted, and the necessary dimensional measurements were made on the samples. ANOVA was applied to determine the most important parameter affecting dimensional accuracy. The ANN model was employed for the numerical prediction of dimensional accuracy in AM-produced parts. This model is commonly favored in nonlinear systems that rely on numerous parameters.

2 | MATERIALS AND METHODS

2.1 | 3D printing process

A fused deposition modeling (FDM) based Creality Ender 6 3D printer was used to fabricate the test samples. The printing volume of the printer is 250 × 250 × 400 mm. In addition, it is capable of 0.1 mm precision, 0.4 mm nozzle diameter, and 150 mm/s printing speed. Creality is a direct-drive printer that uses a 1.75 mm diameter filament. This printer is compatible with many filament materials, such as PLA, ABS, flexible, nylon, conductive, and wood. In this study, 1.75 mm diameter and dark green PLA filament was used in the fabrication of the samples. Three samples of each sample were fabricated to minimize errors that may occur during printing and measurement.

The 3D design process of the proposed model was performed using SolidWorks software. The created design is then saved in the standard triangle language (STL) format and transferred to the slicing program. A slicing program called Cura was used to slice the file in this format. The G-code was created and was ready for printing with the slicing process. The technical drawing and 3D image of the model, which was designed using basic geometries such as cylindrical, triangular, and pentagonal, are shown in Figure 1.

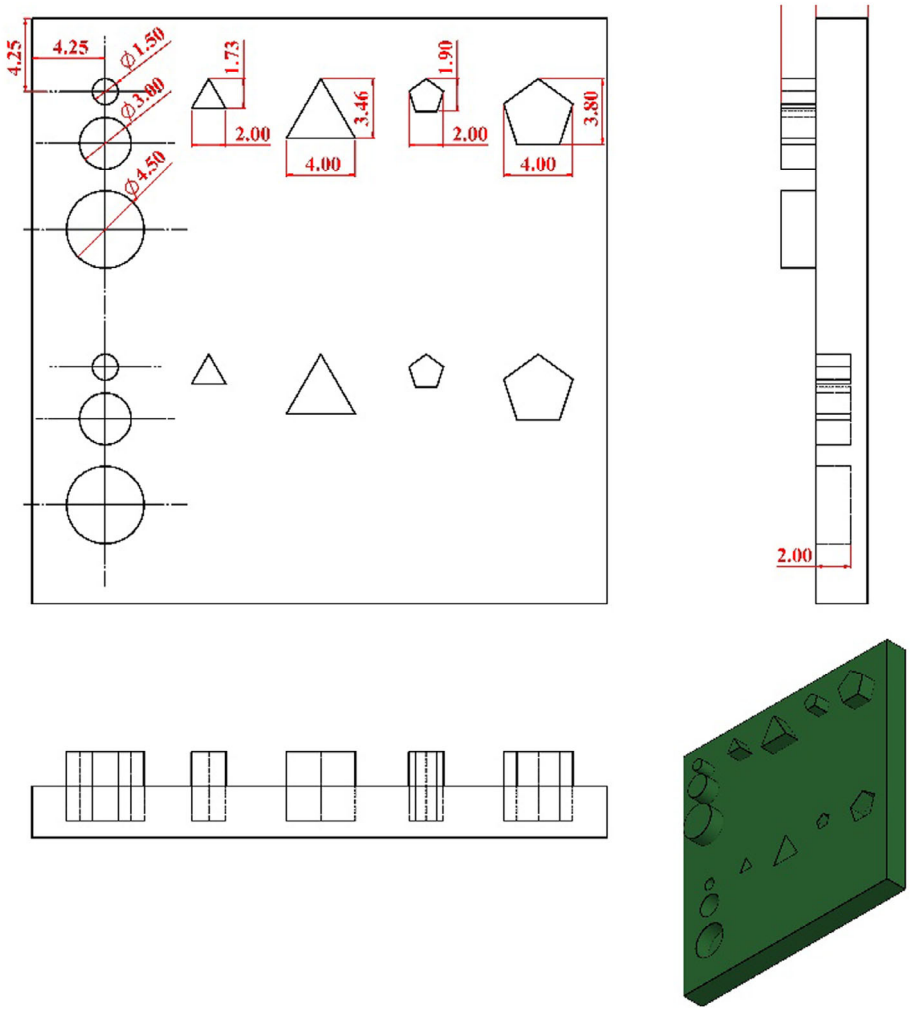

FIGURE 1 Technical drawing and 3D model of the designed sample.

2.2 | Design of the experiment

The experimental design process created to examine the relationship between printing parameters and dimensional accuracy was performed using the Taguchi method. This method is an important application for producing low-cost and high-quality products.[54,55] Taguchi methodology provides complete information on stress factors with a minimum number of experiments. The graphs resulting from this analysis should be considered to determine how the parameters interact. These graphs also show the complexity of the process performance relative to the parameter levels.[56] This study demonstrates the application of the power of experimental design to dimensional accuracy problems. The printing factors and level values are shown in Table 1. The infill pattern, wall thickness (mm), infill density (%), and layer thickness (μm) were selected as printing parameters. There are three levels for each printing parameter in the designed experimental process. While the 3D printing process involves numerous parameters, this study focuses on specific factors that significantly impact the dimensional accuracy of the produced parts. These printing factors and levels were determined from a literature review. The results in Section 3 prove that each printing parameter has an impact on the dimensional accuracy.

The experimental design was made with the Taguchi L9 orthogonal array to obtain the optimum values of the FDM parameters and to minimize the time and cost factors that negatively affect the experimental process. The signal-to-noise (S/N) ratio was used to optimize the determined parameters, ensure stability, and minimum process variability. The experimental design suggested by Taguchi method is shown in Table 2. The number of experiments was reduced from 81 to 9 by using the Taguchi method. The effect of these factors will be fully understood with this number of experiments. Each experiment was repeated three times to obtain the optimum dimensional accuracy.

2.3 | Experimental procedure

In this study, the effect of printing parameters on the dimensional accuracy of three different basic shapes fabricated by the FDM method was examined. Cylindrical pillows of three different sizes, and triangular and pentagonal pieces of two different sizes were used in the model (Figure 1). The developed model is suitable for dimensional accuracy analysis because it includes basic and repeated shapes. Taguchi method determined the fabrication of a total of 27 samples, with three samples produced from each experiment listed in Table 2. The samples fabricated by the FDM method are given in Figure 2.

The dimensions of all samples were measured using a precision digital caliper. As three samples were fabricated, the mean and standard deviation values were calculated for each measurement. These results are given and evaluated in Section 3.1. The effects of printing parameters on the average S/N ratio were determined by Taguchi methodology. The "nominal is best" approach was employed among the criteria used to define S/N values. This approach is useful for analyzing or identifying scaling factors, which are factors in which the mean and standard deviation vary proportionally. The results of the analysis were evaluated in Section 3.2. ANOVA was conducted to analyze the data derived from experimental results, explore interactions among printing parameters, and uncover any differences between them. The results of the ANOVA are given in Section 3.3. Finally, the ANN model was used to predict the test results from the measurements. The details and estimation results about this model were given in Section 3.4.

TABLE 1 The design parameters of the Taguchi method.

	Levels		
Factors	**1**	**2**	**3**
Infill pattern	Cubic	Zigzag	Concentric
Wall thickness (mm)	1	2	3
Infill density (%)	40	70	90
Layer thickness (μm)	100	200	300

3 | RESULTS AND DISCUSSION

3.1 | Evaluation of the measurement results

In this section, the measurement results are evaluated to determine the dimensional accuracy of the samples

TABLE 2 The experiments recommended by the L9 Taguchi method.

	Factors and levels			
Run	**Infill pattern**	**Wall thickness**	**Infill density**	**Layer thickness**
1	Cubic	1	40	100
2	Cubic	2	70	200
3	Cubic	3	90	300
4	Zigzag	1	70	300
5	Zigzag	2	90	100
6	Zigzag	3	40	200
7	Concentric	1	90	200
8	Concentric	2	40	300
9	Concentric	3	70	100

obtained as a result of fabrication with FDM. In addition to dimensional accuracy, the amount of material consumed and the printing time of the part are also important. These values were calculated using Cura, the slicing software for the 3D printer. Consumption and time data recorded using the software are shown in Figure 3A. The highest material consumption was determined as 4.3 g in the 3rd and 9th experiments. The highest printing time was calculated as 33 min in the 9th experiment.

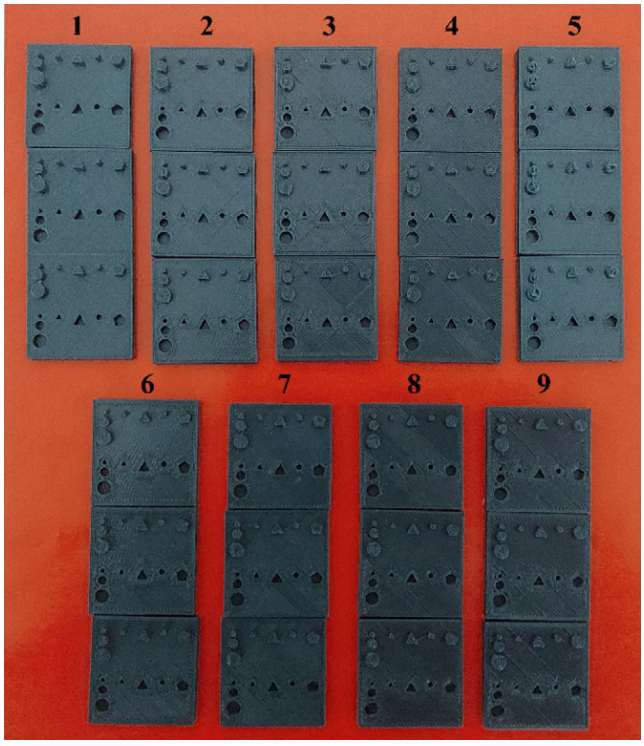

FIGURE 2 3D printed test samples.

The dimensional values of the samples were measured by assigning numbers to each piece. Figure 3A shows the numbers given to the cylindrical, triangular, and pentagonal parts. While the diameters of the cylindrical pillows were measured, the dimensions of the triangular and pentagonal parts in the x-y direction were measured. Because the samples were fabricated in 3 pieces, the mean and standard deviation values were calculated. Table 3 shows the average diameter and standard deviation values of the cylindrical pillows fabricated with different diameters. Tables 4 and 5 show the distance average and standard deviation values of the triangle and pentagon parts on the x-y axis, respectively. The maximum standard deviation values are seen as 0.05 in the tables. The experimental studies can be repeatable since these values are low.

The dimensional deviations of cylindrical pillows modeled in three different diameters are given in percentage terms in Figure 4. Here, pieces 1, 2, and 3 are embossed, and pieces 4, 5, and 6 are debossed. Figure 4A shows the dimensional deviation of the 1.5 mm diameter cylindrical pillow. The deviations between the embossed and debossed parts are different. The reason for the higher deviation amount in the debossed parts is that the parts shrink during fabrication. While the minimum deviation value for the embossed part was observed in experiment 7, it was determined in experiment 8 for the debossed part. The highest dimensional deviation value was observed in experiment 5 with 14.85%. The pieces did not fully emerge in this experiment.

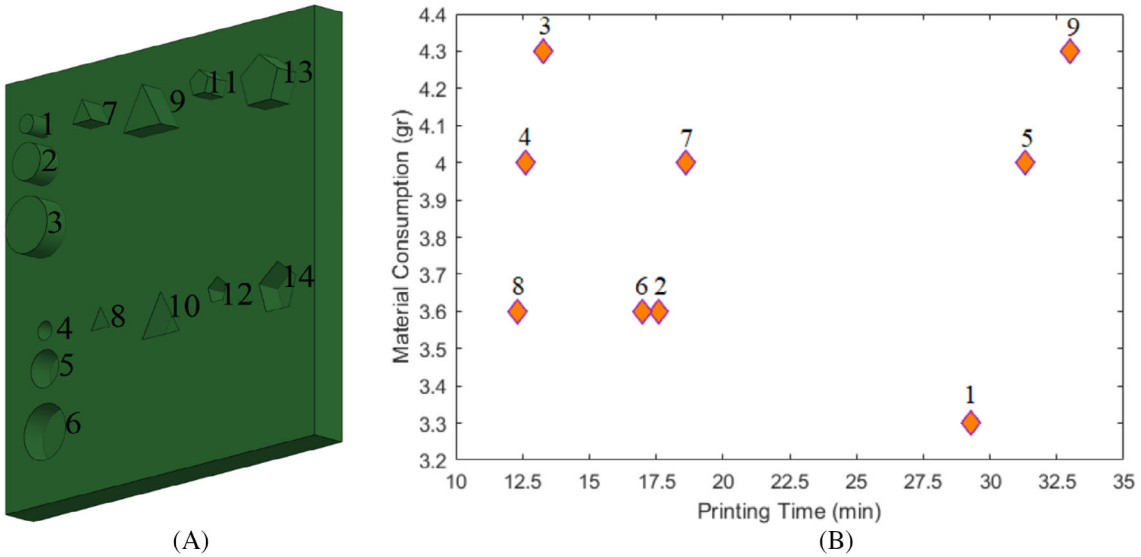

FIGURE 3 Numbering of the model and slicing program outputs. (A) Number of measuring pieces (B) Printing time and material consumption.

TABLE 3 Mean of diameter and standard deviation of the cylindrical pillows.

		Num. Of pieces	1	2	3	4	5	6	7	8	9
1.5 mm dia.	Mean diameter (mm)	1	1.45	1.59	1.63	1.45	1.62	1.61	1.55	1.58	1.62
		4	1.47	1.34	1.29	1.48	1.38	1.41	1.57	1.37	1.49
	Standard deviation (mm)	1	0.04	0.01	0.01	0.03	0.04	0.03	0.05	0.03	0.05
		4	0.05	0.05	0.05	0.05	0.05	0.05	0.03	0.05	0.05
3 mm dia.	Mean diameter (mm)	2	3.02	3.12	3.03	2.96	3.03	2.98	3.06	2.99	2.96
		5	2.65	2.56	2.59	2.70	2.77	2.69	2.66	2.59	2.81
	Standard deviation (mm)	2	0.04	0.05	0.01	0.02	0.05	0.05	0.05	0.04	0.05
		5	0.05	0.05	0.05	0.05	0.05	0.04	0.05	0.05	0.05
4.5 mm dia.	Mean diameter (mm)	3	4.48	4.60	4.58	4.49	4.47	4.52	4.44	4.45	4.40
		6	4.31	4.24	4.19	4.29	4.39	4.20	4.37	4.24	4.43
	Standard deviation (mm)	3	0.01	0.04	0.02	0.03	0.02	0.02	0.01	0.02	0.02
		6	0.05	0.02	0.03	0.02	0.05	0.05	0.04	0.04	0.04

TABLE 4 Mean of distance and standard deviation in the x-axis of polygonal pieces.

		Num. of pieces	1	2	3	4	5	6	7	8	9
2 mm triangle	Mean diameter (mm)	7	1.73	1.69	1.65	1.57	1.56	1.65	1.57	1.58	1.71
		8	1.94	1.88	1.94	1.99	1.93	1.87	1.88	1.94	1.90
	Standard deviation (mm)	7	0.03	0.01	0.03	0.01	0.05	0.04	0.03	0.02	0.01
		8	0.02	0.05	0.01	0.01	0.04	0.03	0.01	0.02	0.04
4 mm triangle	Mean diameter (mm)	9	3.59	3.56	3.64	3.61	3.69	3.60	3.56	3.61	3.69
		10	3.93	3.90	3.95	4.00	3.76	3.85	3.84	3.94	3.71
	Standard deviation (mm)	9	0.04	0.01	0.01	0.01	0.02	0.02	0.02	0.01	0.04
		10	0.02	0.02	0.04	0.01	0.04	0.01	0.01	0.02	0.02
2 mm pentagon	Mean diameter (mm)	11	1.92	1.56	1.62	1.91	1.77	1.56	1.68	1.55	1.76
		12	2.02	1.74	1.72	2.01	1.76	1.64	1.74	1.80	1.83
	Standard deviation (mm)	11	0.05	0.05	0.05	0.05	0.05	0.05	0.05	0.05	0.05
		12	0.05	0.05	0.05	0.05	0.05	0.04	0.05	0.05	0.05
4 mm pentagon	Mean diameter (mm)	13	3.97	3.17	3.15	3.31	3.35	3.10	3.14	3.16	3.01
		14	3.74	3.43	3.37	3.58	3.60	3.42	3.56	3.40	3.52
	Standard deviation (mm)	13	0.05	0.04	0.05	0.05	0.05	0.05	0.05	0.03	0.05
		14	0.05	0.01	0.01	0.05	0.02	0.05	0.02	0.05	0.01

The deviations of the 3 mm diameter cylindrical pillows are shown in Figure 4B. Here, part 2 is embossed and part 5 is debossed. There was a significant difference in the amount of deviation between the two parts. The debossed part has shrunk during fabrication and is far from the actual value. While the minimum deviation value for the embossed part was observed in experiment 8, it was determined in experiment 9 for the debossed part. The highest dimensional deviation value, 14.60%, occurred in piece 5 in experiment 2.

The deviations of the 4.5 mm diameter cylindrical pillows are given in Figure 4C. Here, part 3 is embossed and part 6 is debossed. Although there are deviation values between two parts that are close to each other, the deviation amounts are different in many experiments. While the minimum deviation value for the embossed part was observed in experiment 4, it was determined in experiment 9 for the debossed part. The highest deviation value, 6.89%, occurred in piece 6 in experiment 3. The deviation values decreased as the hole diameters of the

TABLE 5 Mean of distance and standard deviation in the y-axis of polygonal pieces.

		Num. of pieces	1	2	3	4	5	6	7	8	9
2 mm triangle	Mean diameter (mm)	7	1.59	1.53	1.51	1.51	1.50	1.55	1.51	1.46	1.63
		8	1.86	1.84	1.84	1.78	1.89	1.85	1.83	1.83	1.87
	Standard deviation (mm)	7	0.05	0.01	0.03	0.03	0.04	0.05	0.02	0.04	0.01
		8	0.05	0.05	0.01	0.02	0.04	0.04	0.05	0.05	0.05
4 mm triangle	Mean diameter (mm)	9	3.17	3.24	3.18	3.26	3.22	3.20	3.23	3.28	3.25
		10	3.73	3.68	3.73	3.72	3.63	3.68	3.61	3.64	3.58
	Standard deviation (mm)	9	0.04	0.05	0.01	0.05	0.03	0.02	0.05	0.04	0.05
		10	0.02	0.02	0.03	0.04	0.04	0.05	0.01	0.03	0.03
2 mm pentagon	Mean diameter (mm)	11	1.86	1.73	1.62	1.93	1.67	1.64	1.70	1.61	1.47
		12	2.08	1.48	1.74	2.00	1.86	1.84	1.74	1.73	1.76
	Standard deviation (mm)	11	0.04	0.05	0.05	0.05	0.05	0.05	0.05	0.05	0.05
		12	0.05	0.02	0.04	0.05	0.05	0.05	0.05	0.04	0.05
4 mm pentagon	Mean diameter (mm)	13	3.34	2.81	2.86	2.90	3.09	3.05	2.98	2.74	2.96
		14	3.59	3.46	3.26	3.55	3.54	3.36	3.54	3.36	3.54
	Standard deviation (mm)	13	0.05	0.05	0.05	0.05	0.05	0.05	0.05	0.05	0.05
		14	0.05	0.04	0.05	0.04	0.03	0.05	0.05	0.05	0.05

cylindrical pillows increased (Figure 4). The lowest standard deviation values were measured on a 4.5 mm diameter cylindrical pillow. The experiment in which the highest deviation value was measured among the cylindrical pillows was experiment 3.

The dimensional deviations of the triangular parts in the x and y-axes are shown in percentage terms in Figure 5. Here, parts 7 and 9 are embossed, and parts 8 and 10 are debossed. Figure 5A shows the dimensional changes of 2 mm wide triangular pieces on the x-axis. The deviations between the embossed and debossed parts were different. This difference is quite high, especially in experiment 5. The reason for the high deviation of debossed parts is the dimensional reduction that occurs during fabrication. The highest deviation amount was calculated as 27.12% in the debossed part 8 in experiment 5. The lowest deviation was determined as 0.51% for embossed piece 7 in experiment 4.

Figure 5B shows the dimensional change of the 2 mm wide triangular pieces on the y-axis. Part 7 is embossed and part 8 is debossed. The amount of deviation between the parts is different. The minimum deviation in the y-axis was observed in experiment 9 for the debossed triangular parts. However, the minimum deviation in the y-axis was determined in experiment 5 for the embossed triangular parts. The highest deviation in the y-axis occurred in piece 8 in experiment 3, with 18.5%.

Figure 5C shows the dimensional changes of the 4 mm wide triangular pieces on the x-axis. The deviation amounts of the debossed and embossed triangle parts on the x-axis are different from each other. Here, the results are similar to the x-axis deviation values of 2 mm triangular pieces. However, there is a significant decrease in the percentage deviation as the width of the triangular piece increases. The minimum deviation in the x-axis occurred in the embossed piece 9 in experiment 4, as in the 2 mm piece. The highest deviation in the x-axis occurred in piece 10 in experiment 2, with 11.5%.

Figure 5D shows the dimensional changes of the 4 mm wide triangular pieces on the y-axis. The deviations between the debossed and embossed parts are different. For triangle piece 9 that is embossed, the minimum deviation in the y-axis is observed in experiment 9, whereas for triangle piece 10 that is debossed, the minimum deviation in the y-axis is seen in experiment 8, as in 2 mm wide triangle pieces. For the 4 mm triangular piece, the highest deviation in the y-axis was 8.15%, occurring in piece 10 in experiment 1. In the case of the x-axis, enlarging the part width along the y-axis resulted in a decrease in error.

The dimensional deviations of the pentagonal parts in the x and y-axes are shown in percentage terms in Figure 6. Here, parts 11 and 13 are embossed, and parts 12 and 14 are debossed. Figure 6A shows the dimensional changes of 2 mm wide pentagonal pieces on the x-axis. The deviations between the embossed and debossed parts were different. Similar to the triangular parts, there is a significant difference between the

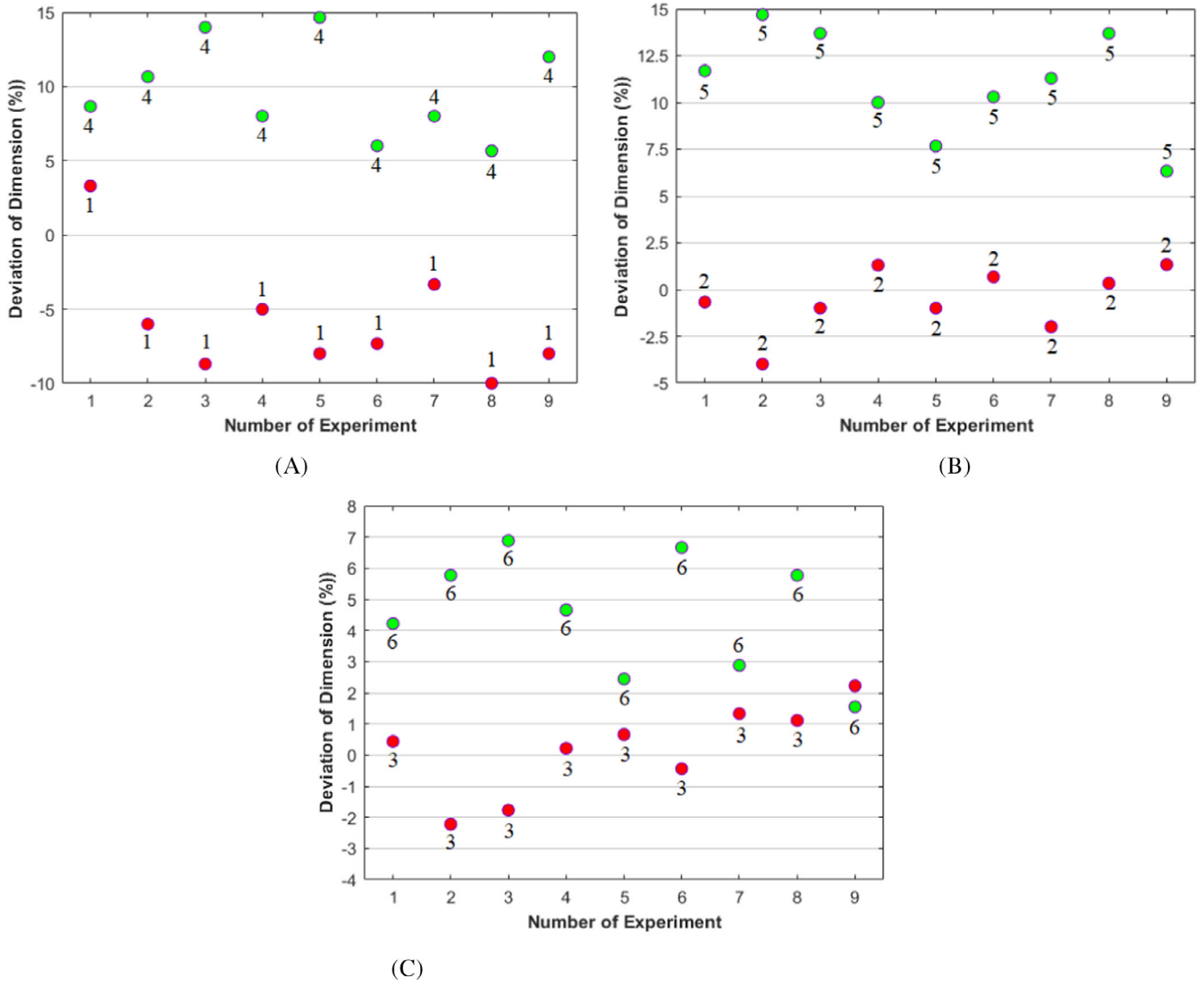

FIGURE 4 Dimensional deviations of cylindrical pillows of different diameters. (A) 1.5 mm diameter cylindrical pillow (B) 3 mm diameter cylindrical pillow (C) 4.5 mm diameter cylindrical pillow.

deviation values. The reason for the high deviation of debossed parts is the dimensional reduction that occurs during fabrication. The highest dimensional deviation was calculated as 22.19% in the debossed part 12 in experiment 8. The lowest amount of deviation was determined as 6.78% in embossed piece 11 in experiment 1.

Figure 6B shows the dimensional change of the 2 mm wide pentagonal pieces on the y-axis. Part 11 is embossed and part 12 is debossed. The amount of deviation between the parts is noticeable. The minimum deviation in the y-axis was observed in experiment 5 for the embossed pentagonal parts. However, the minimum deviation in the y-axis was determined in experiment 4 for the debossed pentagonal parts. The highest deviation with 17.5% in the y-axis occurred in piece 12 in experiment number 9.

Figure 6C shows the dimensional changes of the 4 mm wide pentagonal pieces in the x-axis. While the parts 13 here are embossed, the parts 14 are debossed. The deviations of 4 mm pieces are lower than those of 2 mm pieces. The highest deviation value appeared in debossed pentagonal parts. The highest deviation value in the x-axis of the 4 mm pentagonal piece occurred in the debossed piece 14 in experiment 9. This deviation value is approximately 24.90%. The lowest amount of deviation occurred with 5.81% in piece number 13 in experiment 1.

Figure 6D shows the dimensional changes of the 4 mm wide pentagonal pieces on the y-axis. There is a significant difference between the deviation values of the debossed and embossed parts as seen in other measurements. For pentagon pieces 13 that are embossed, the minimum deviation in the y-axis is seen in experiment 1, while for triangle pieces 14 that are debossed, the minimum deviation in the y-axis is seen in experiment 1, as in 2 mm wide pentagon pieces. The highest deviation in the

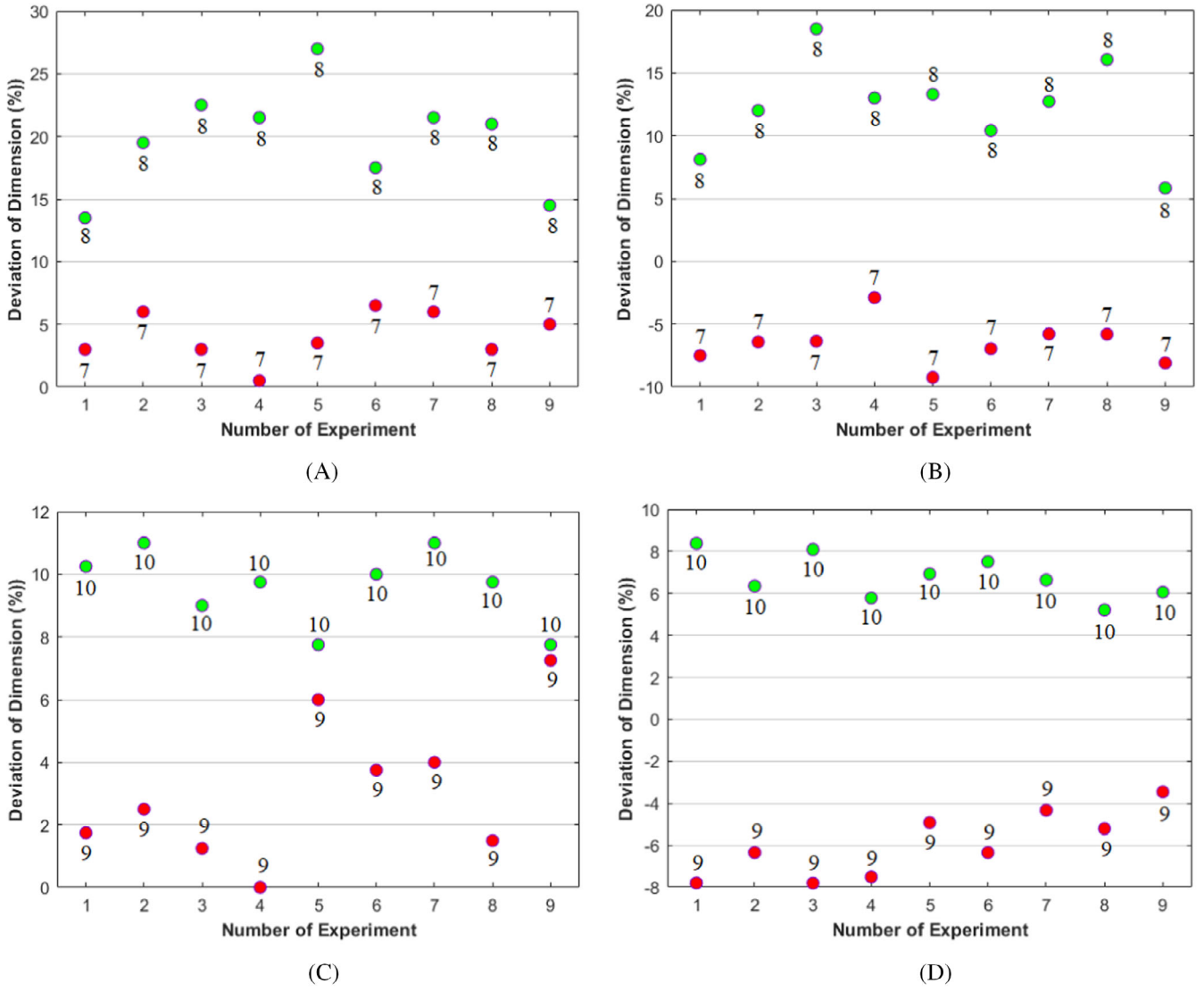

FIGURE 5 Deviation of triangle pieces in the x and y axes. (A) 2 mm wide triangle pieces in the x-axis (B) 2 mm wide triangle pieces in the y-axis (C) 4 mm wide triangle pieces in the x-axis (D) 4 mm wide triangle pieces in the y-axis.

y-axis occurred in piece 14 in experiment 8, with 27.58% for the 4 mm pentagonal piece.

3.2 | Evaluation of the Taguchi method results

In this study, Taguchi methodology was performed with Minitab 16, a statistical software. This analysis was performed for each part whose measurements are given in Section 3.1. The effects of printing parameters on the average S/N ratio were determined through analysis. Optimization, stability, and minimum process variability of printing parameters can be achieved with this ratio. The effect results of printing parameters on the average SN ratio for dimensional accuracy are given in Figures 7–12. 1, 2, and 3 correspond to the levels in Table 1. For the infill pattern, 1, 2, and 3 correspond to cubic, zigzag, and concentric levels, respectively, while, 1, 2, and 3 indicate levels of 1, 2, and 3 mm, for wall thickness. Besides, 1, 2, and 3 correspond to 40%, 70%, and 90% levels for infill density. Finally, for layer thickness, 1, 2, and 3 indicate levels of 100, 200, and 300 μm, respectively.

First, the effect of printing parameters on material consumption and printing time was analyzed. Figure 7 shows the effect of the parameters for the samples on the average SN rate for material consumption and printing time. The best results for material consumption were obtained with a concentric infill pattern, 3 mm wall thickness, 90% infill density and 300 μm layer thickness (Figure 7A). However, the most effective parameter for material consumption is the infill density. Increasing the infill density significantly increases material

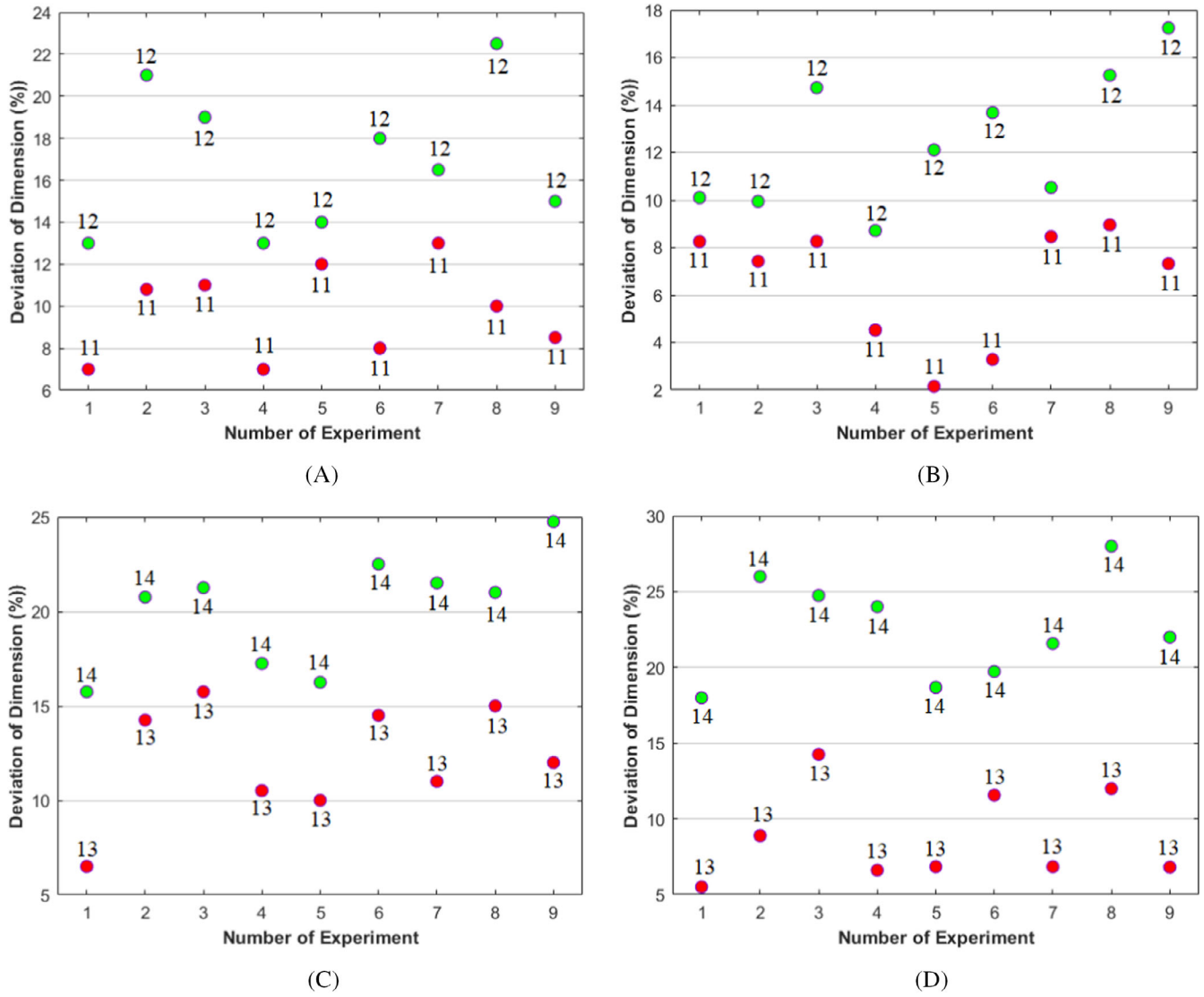

FIGURE 6 Deviation of pentagon pieces in the x and y axes. (A) 2 mm wide pentagon pieces in the x-axis (B) 2 mm wide pentagon pieces in the y-axis (C) 4 mm wide pentagon pieces in the y-axis (D) 4 mm wide pentagon pieces in the y-axis.

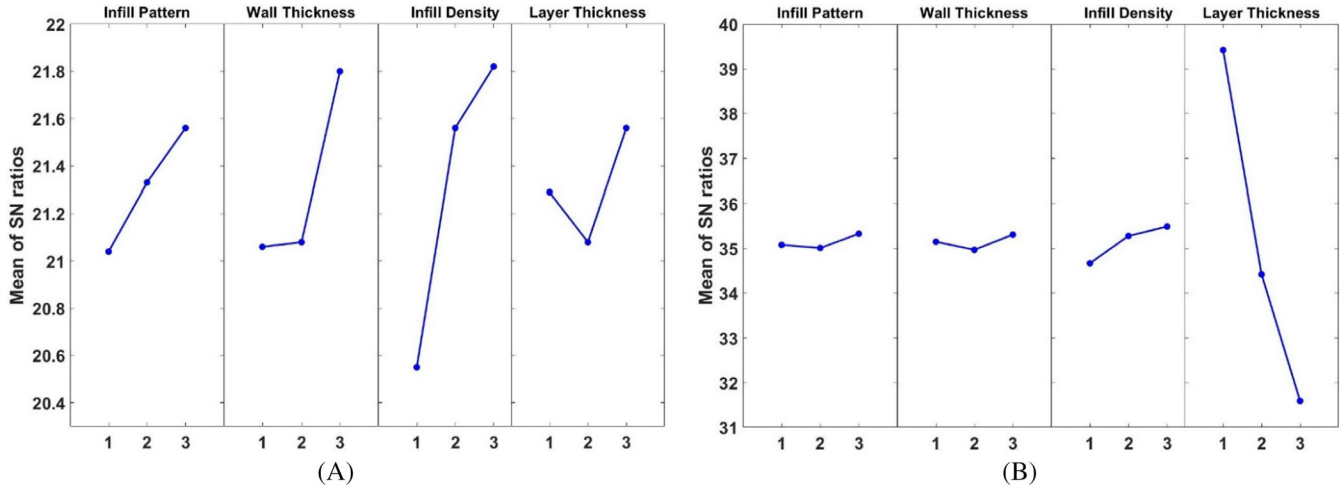

FIGURE 7 Main effects plot for SN ratios (A) material consumption (B) printing time.

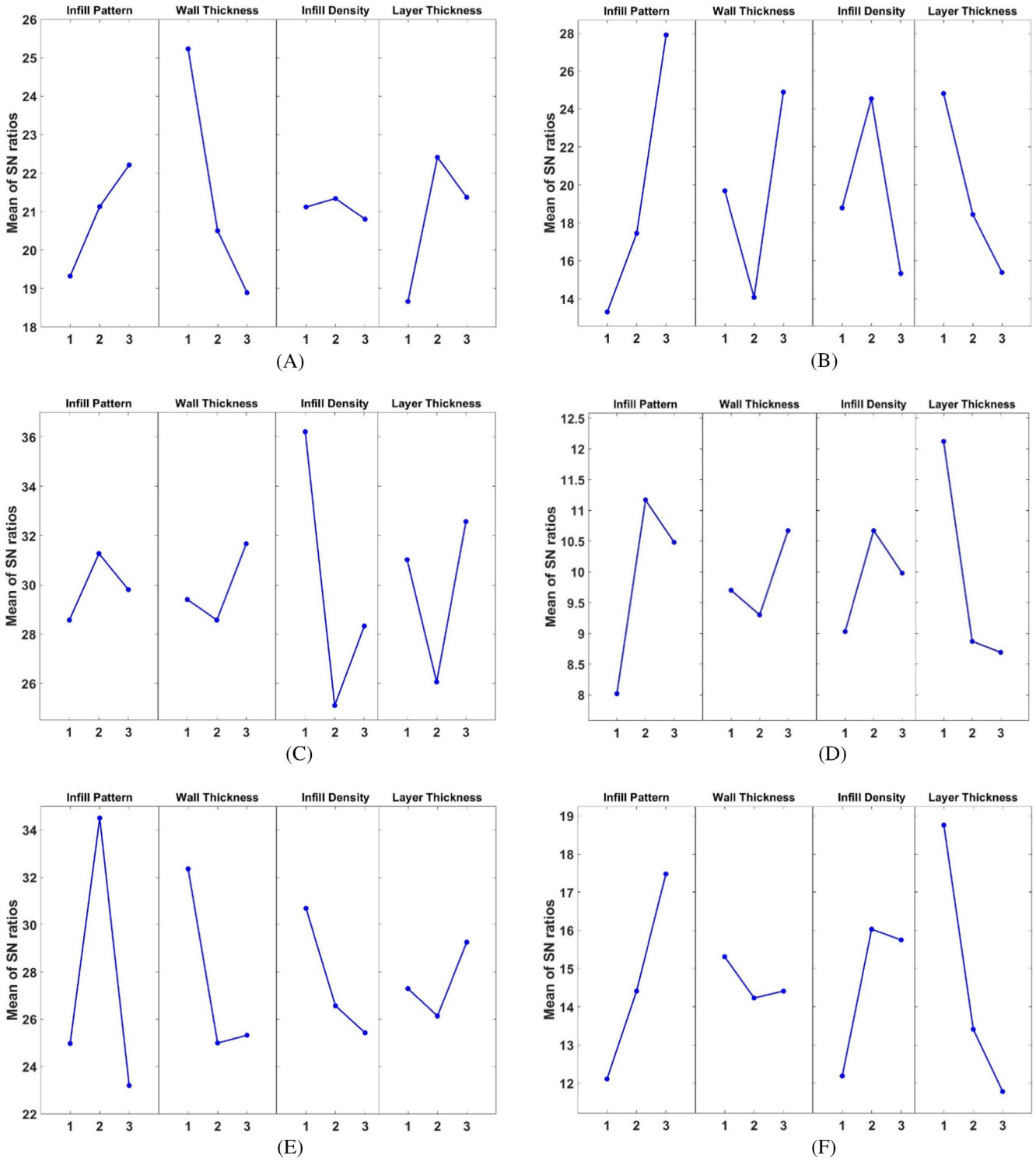

FIGURE 8 Effect of printing parameters on the average SN ratio for 1.5, 3, and 4.5 mm diameter cylindrical pillows. (A) Number 1 cylindrical pillow with a diameter of 1.5 mm (B) Number 4 cylindrical pocket with a diameter of 1.5 mm (C) Number 2 cylindrical pillow with a diameter of 3 mm (D) Number 5 cylindrical pocket with a diameter of 3 mm (E) Number 3 cylindrical pillow with a diameter of 4.5 mm (F) Number 6 cylindrical pocket with a diameter of 4.5 mm.

consumption. The best printing time results were obtained with a concentric infill pattern, 3 mm wall thickness, 90% infill density and 100 μm layer thickness (Figure 7B). However, the most effective parameter for material consumption is the layer thickness. Decreasing the layer thickness parameter increases the printing time.

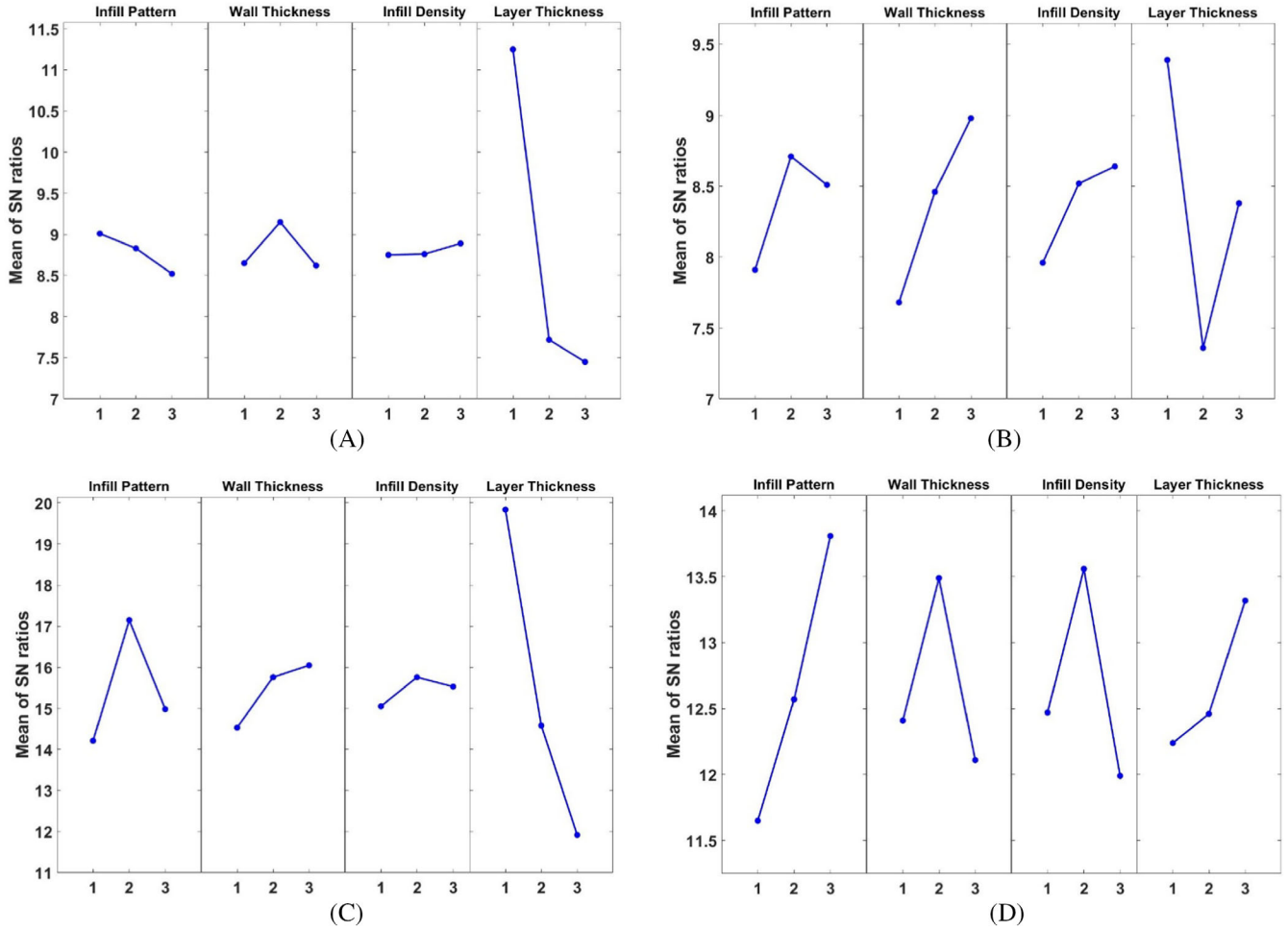

FIGURE 9 Effect of printing parameters on the average SN ratio for the x and y axes of the 2 mm wide triangular pieces. (A) Number 7 triangular part with a wide of 2 mm (x-axis) (B) Number 8 triangular part with a wide of 2 mm (x-axis) (C) Number 7 triangular part with a wide of 2 mm (y-axis) (D) Number 8 triangular part with a wide of 2 mm (y-axis).

Figure 8 shows the effect of printing parameters on the average SN ratio for the dimensional accuracy of cylindrical pillows. The analysis results varied depending on the size of each cylindrical pillow and whether it was debossed or embossed. The best results for embossed parts (Figure 8A–E) were obtained with a zigzag-concentric infill pattern, 1–3 mm wall thickness, 40%–70% infill density and 200–300 μm layer thickness. However, the most effective parameters for the dimensional accuracy of embossed parts are the infill pattern and density. The best results for debossed parts (Figure 8B–F) were obtained with a zigzag-concentric infill pattern, 1–3 mm wall thickness, 70% infill rate and 100 μm layer thickness. However, the most effective parameters for the dimensional accuracy of the debossed parts appear to be the infill pattern and layer thickness. The most important parameter affecting the dimensional accuracy of cylindrical pillows is the infill pattern. If a cylindrical pillow with high accuracy is desired to be fabricated, the infill pattern must be selected correctly.

Figure 9 shows the effect of printing parameters on the average SN ratio for the dimensional accuracy of the x and y axes of the 2 mm wide triangular pieces. For the embossed part (Figure 9A–C), the best results were obtained with a cubic-zigzag infill pattern, a wall thickness of 2–3 mm, 70%–90% infill density and 100 μm layer thickness. The layer thickness is the parameter that primarily influences the dimensional accuracy of part 7 in both the x and y planes. The parameters affecting the dimensional accuracy of the debossed parts were different. The best results for debossed parts (Figure 9B–D) were obtained with a zigzag-concentric infill pattern, 2–3 mm wall thickness, 70%–90% infill density and 100–300 μm layer thickness. The parameters with the greatest impact on the dimensional accuracy of part 8 in both the x and y-planes are the infill pattern and layer thickness. The effect of the layer thickness parameter on the dimensional accuracy of 2 mm wide triangular parts was quite high. Triangular parts were fabricated with high accuracy at low layer thickness.

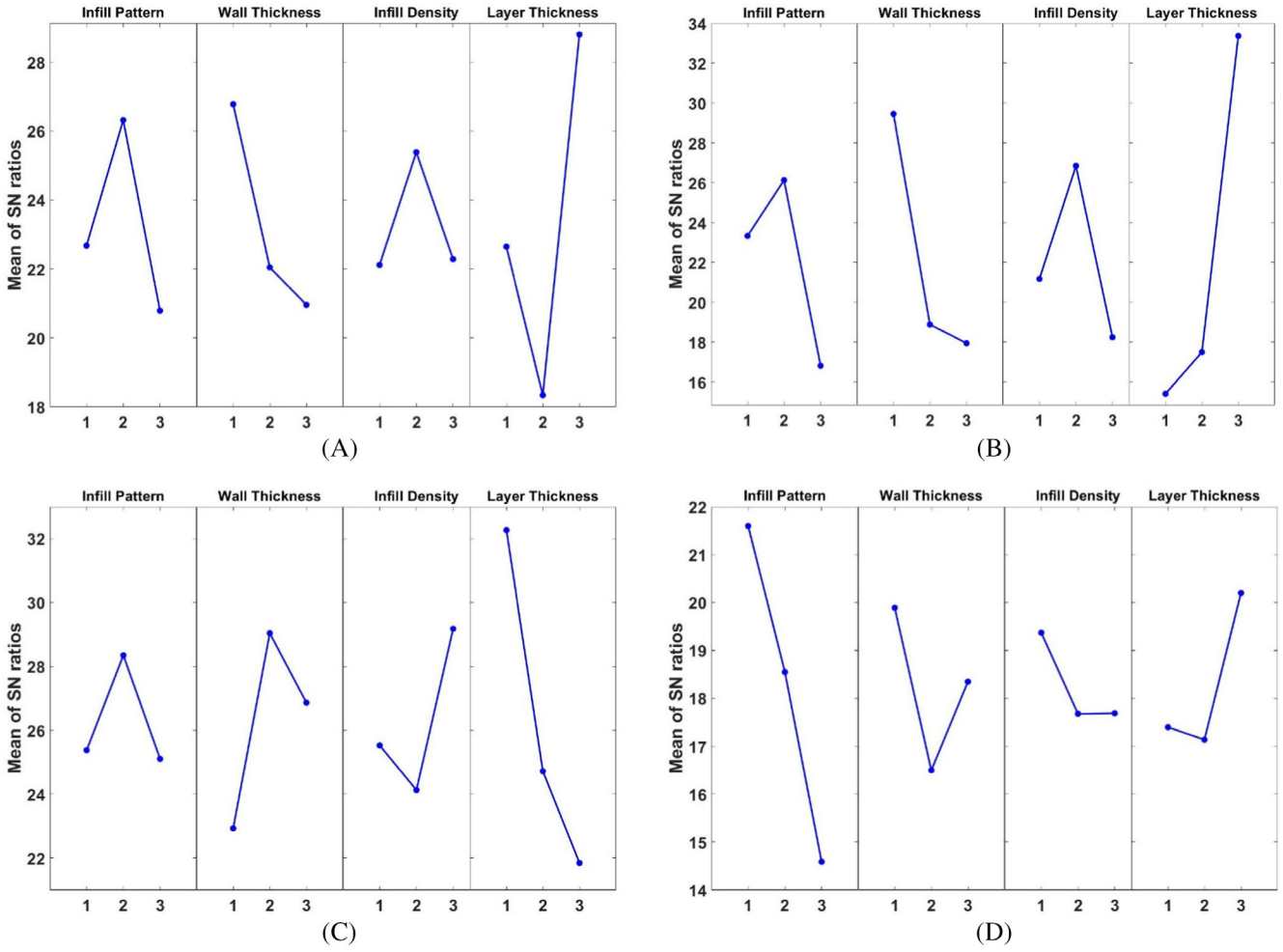

FIGURE 10 Effect of printing parameters on the average SN ratio for the x and y axes of the 4 mm wide triangular pieces. (A) Number 9 triangular part with a wide of 4 mm (x-axis) (B) Number 10 triangular part with a wide of 4 mm (x-axis) (C) Number 9 triangular part with a wide of 4 mm (y-axis) (D) Number 10 triangular part with a wide of 4 mm (y-axis).

Figure 10 shows the effect of printing parameters on the average SN ratio for the dimensional accuracy of the x and y-axes of the 4 mm wide triangular pieces. As expected, similar results were observed with the results obtained in 2 mm triangular pieces (Figure 9). Changing the part size did not change the effect of the printing parameters. The best results for the embossed part (Figure 10A–C) were obtained with a zigzag infill pattern, 1–2 mm wall thickness, 70%–90% infill ratio and 100–300 μm layer thickness. The layer thickness is the parameter that predominantly influences the dimensional accuracy of part 9 in both the x and y-planes. The best results for debossed parts (Figure 10B–D) were obtained with a cubic-zigzag infill pattern, 1 mm wall thickness, 40%–70% infill density and 300 μm layer thickness. The parameters that most affect the dimensional accuracy of part 10 in the *x* and *y*-planes are the infill pattern and layer thickness. As a result, layer thickness was the most effective parameter in 4 mm wide triangular pieces as well as in 2 mm wide triangular pieces. To achieve high dimensional accuracy in triangular parts, the layer thickness value must be selected correctly.

Figure 11 shows the effect of printing parameters on the average SN ratio for the dimensional accuracy of the x and y-axes of the 2 mm wide pentagon pieces. For the embossed part (Figure 11A–C), the best results were obtained with a zigzag-concentric infill pattern, 1 mm wall thickness, 70%–90% infill ratio and 100–200 μm layer thickness. The parameters that most affect the dimensional accuracy of part 11 in the x and y-planes are wall thickness and infill density. The parameters affecting the dimensional accuracy of the debossed parts were different. The best results for debossed parts (Figure 11B–D) were obtained with a cubic infill pattern, 1 mm wall thickness, 40% filling rate and 100 μm layer thickness. It was determined that the parameters most influencing the dimensional accuracy of part 12 in the x and y-planes are the wall and layer thickness. It was determined that the

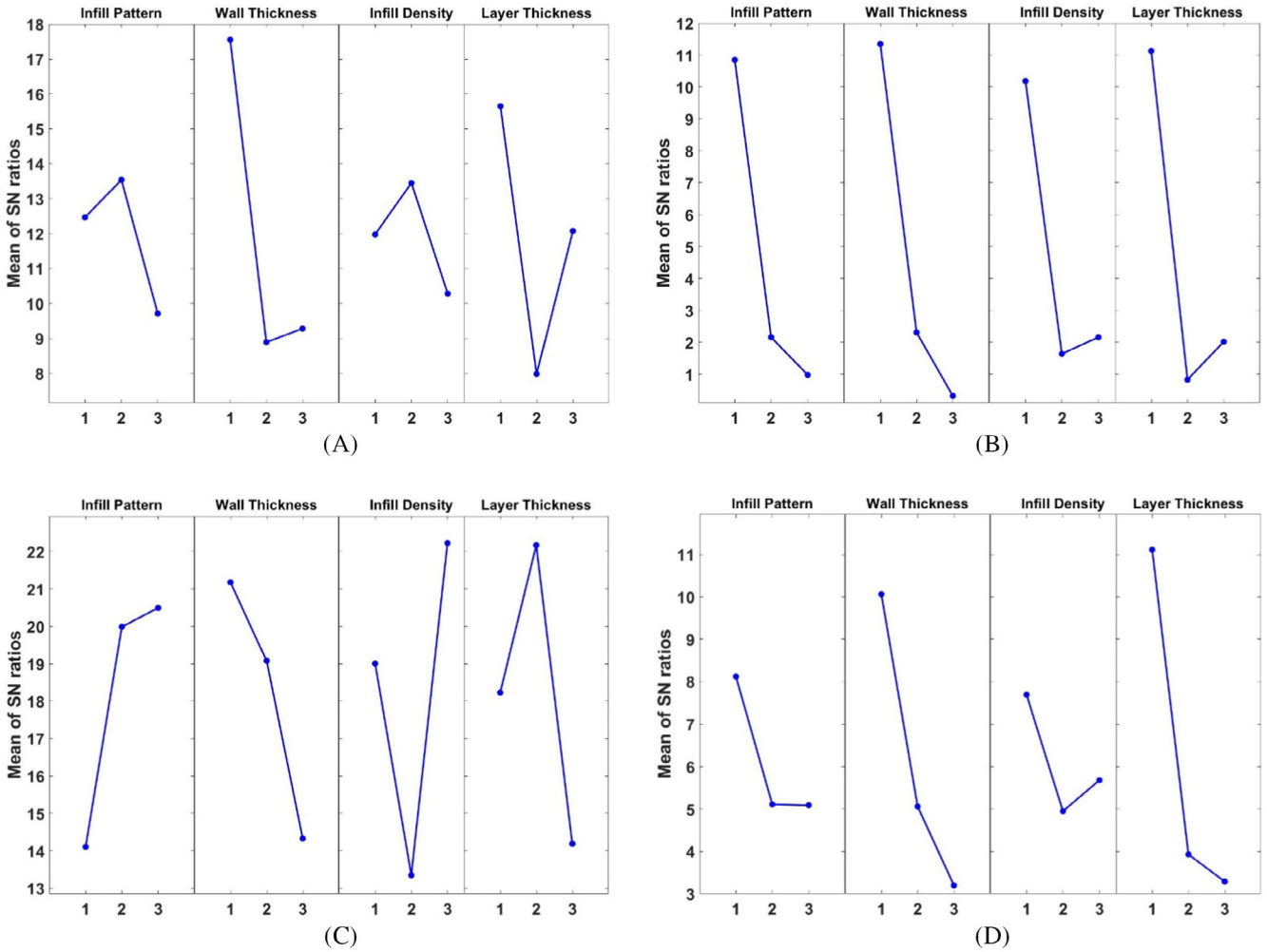

FIGURE 11 Effect of printing parameters on the average SN ratio for the x and y axes of the 2 mm wide pentagon pieces. (A) Number 11 pentagon part with a wide of 2 mm (x-axis) (B) Number 12 pentagon part with a wide of 2 mm (x-axis) (C) Number 11 pentagon part with a wide of 2 mm (y-axis) (D) Number 12 pentagon part with a wide of 2 mm (y-axis).

most important parameter affecting the dimensional accuracy of 2 mm wide pentagon parts is the wall thickness. Pentagon parts were fabricated with high dimensional accuracy at low wall thickness.

Figure 12 gives the effect of printing parameters on the average SN ratio for the dimensional accuracy of x and y-axes of the 4 mm wide pentagon pieces. As expected, similar results were observed with the results obtained with 2 mm pentagon pieces (Figure 11). Changing the part size did not change the effect of the printing parameters. For the embossed part (Figure 12A–C), the best results were obtained in a zigzag infill pattern, 1–3 mm wall thickness, 70%–90% infill ratio and 100–300 μm layer thickness. It was determined that the parameters most influencing the dimensional accuracy of part 13 in the *x* and *y*-planes are the infill pattern and wall thickness. The best results for debossed parts (Figure 12B–D) were obtained with a cubic-zigzag infill pattern, 1 mm wall thickness, 40%–70% infill ratio and 100 μm layer thickness. It was determined that the parameters exerting the most significant influence on the dimensional accuracy of part 14 in both the x and y planes are the wall thickness and layer thickness. The wall thickness was the most effective parameter in 4 mm wide pentagon pieces as well as in 2 mm wide pentagon pieces. To achieve high dimensional accuracy in pentagon parts, the wall thickness value must be selected correctly.

3.3 | Evaluation of the ANOVA results

The analysis of variance (ANOVA) test is a statistical analysis method used to compare the averages between at least three groups. In the analysis phase, we have a categorical variable that has at least three groups and the observations are independent.[57] There must also be a

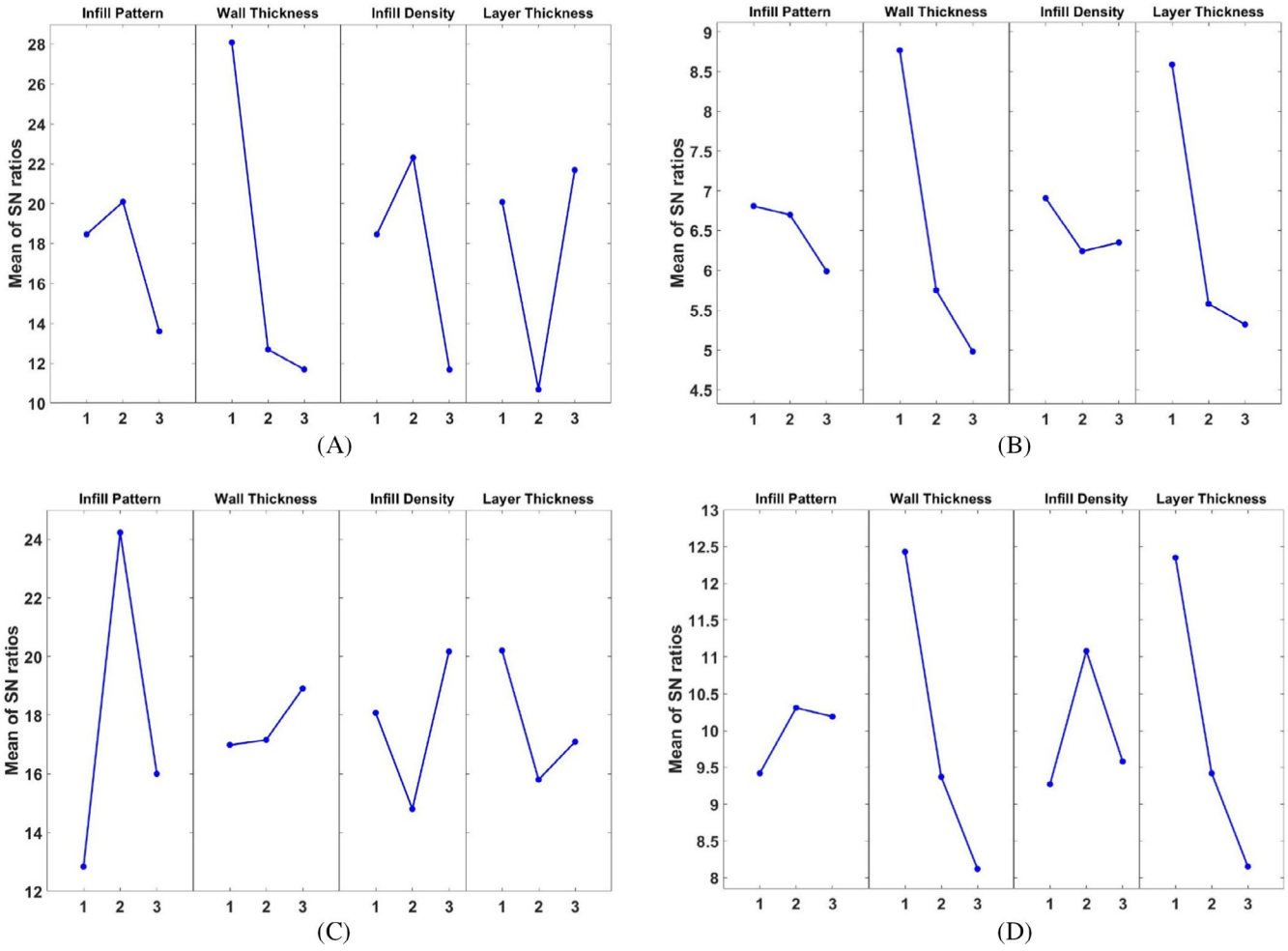

FIGURE 12 Effect of printing parameters on the average SN ratio for the x and y axes of the 4 mm wide pentagon pieces. (A) Number 13 pentagon part with a wide of 4 mm (x-axis) (B) Number 14 pentagon part with a wide of 4 mm (x-axis) (C) Number 13 pentagon part with a wide of 4 mm (y-axis) (D) Number 14 pentagon part with a wide of 4 mm (y-axis).

quantitative variable consisting of numerical data. In this study, ANOVA was used to analyze the data obtained from the experimental results, examine the interaction between printing parameters, and reveal the differences between them. The results of the contribution ratios of printing parameters for dimensional accuracy in the ANOVA table are given in the following graphs (Figures 13–18). The effects of the four different printing parameters on each part are revealed in the figures.

First, the effect of printing parameters on material consumption and printing time was analyzed. Figure 13 shows the effect of printing parameters on material consumption and printing time for the samples. The most effective parameter in material consumption was the infill density of 58.32% (Figure 13A). Increasing this parameter increases material consumption. The least effective parameters were the infill pattern and layer thickness. The effect of the wall thickness parameter was 25.01%. The effect of the layer thickness parameter on the printing time is quite high (Figure 13B). The effect of other parameters was approximately 5% or less.

Figure 14 shows the contribution of the printing parameters to the dimensional accuracy of the cylindrical pillows. The effects of the parameters varied depending on the size of the cylindrical pillows and whether they were debossed or embossed. Among the embossed parts (Figure 14A–E), the most effective parameter for dimensional accuracy is the wall thickness, which is 62.68%. The effect of the printing parameters differed depending on the size of the part. The most effective parameters for embossed cylindrical pillows with diameters of 1.5, 3, and 4.5 mm were wall thickness, infill density, and infill pattern, respectively. Among debossed parts (Figure 14B–F), the most effective parameter for dimensional accuracy is layer thickness, which is 41.46%. The effect of the printing parameters differed depending on the part size. The infill pattern and layer thickness were found to be

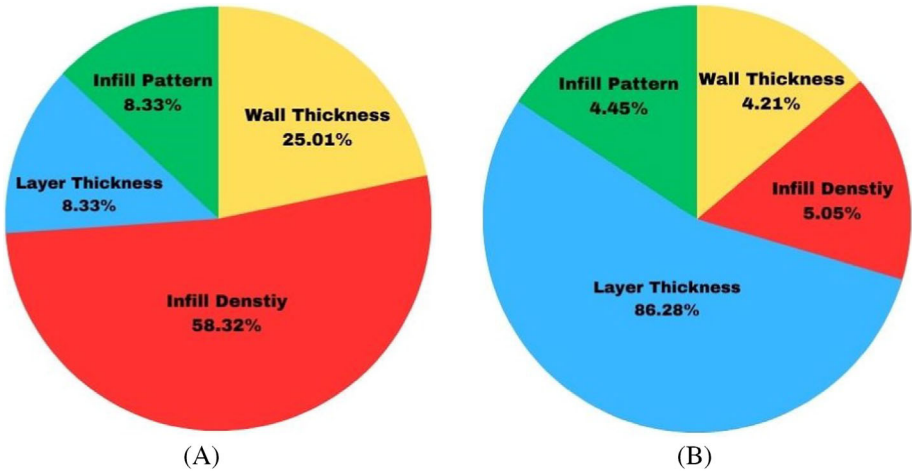

FIGURE 13 Contribution of each parameter for (A) material consumption (B) printing time.

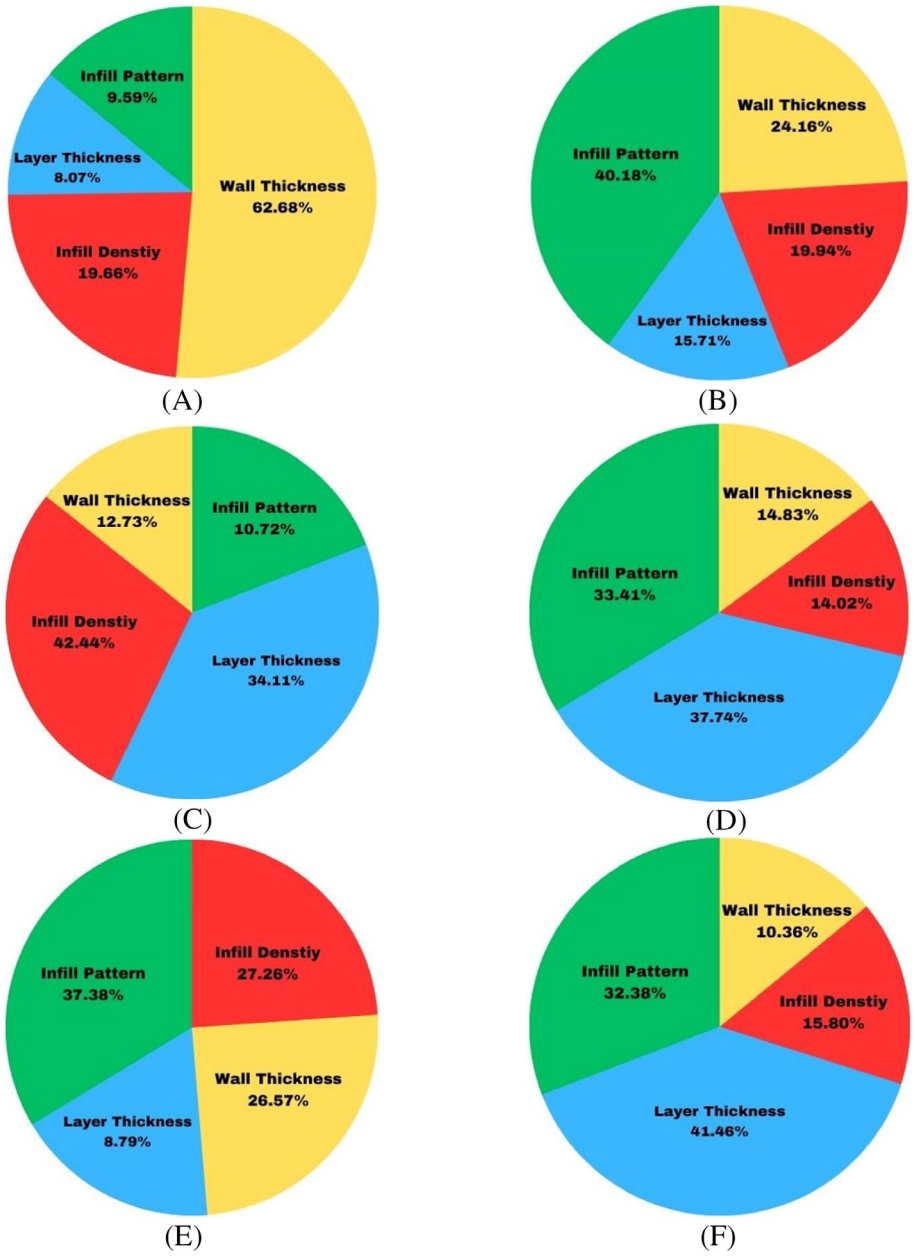

FIGURE 14 Contribution of each parameter for 1.5, 3, and 4.5 mm diameter cylindrical pillows. (A) Number 1 cylindrical pillow with a diameter of 1.5 mm (B) Number 4 cylindrical pocket with a diameter of 1.5 mm (C) Number 2 cylindrical pillow with a diameter of 3 mm (D) Number 5 cylindrical pocket with a diameter of 3 mm (E) Number 3 cylindrical pillow with a diameter of 4.5 mm (F) Number 6 cylindrical pocket with a diameter of 4.5 mm.

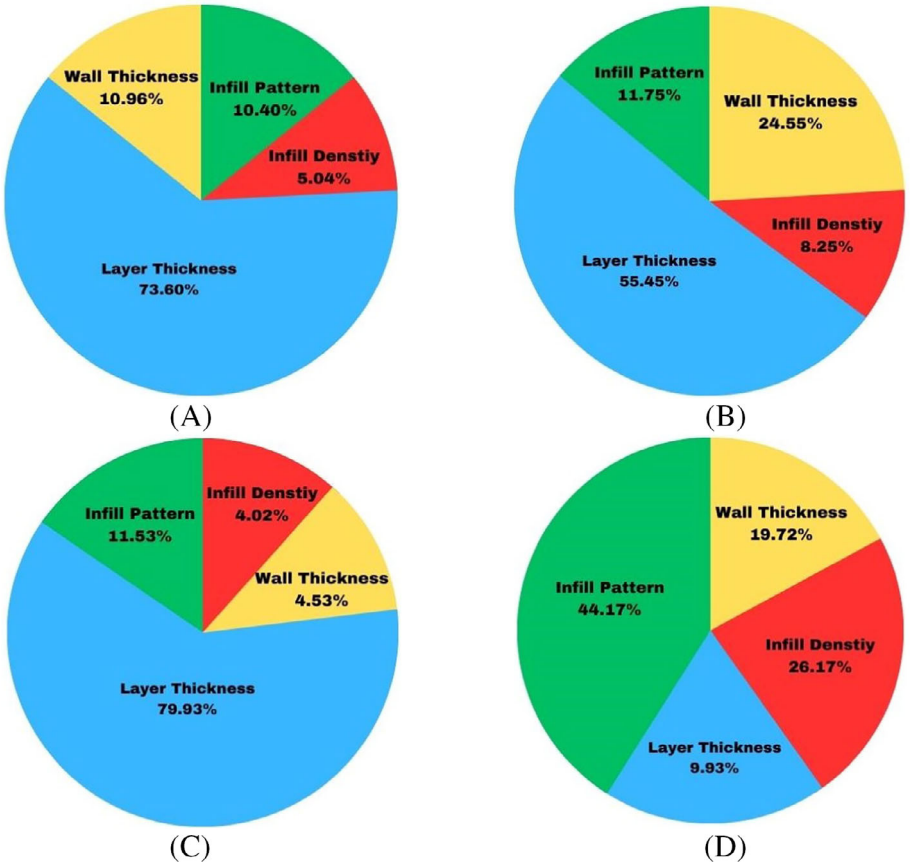

FIGURE 15 Contribution of each parameter for the x and y-axes of the 2 mm wide triangular pieces. (A) Number 7 triangular part with a wide of 2 mm (x-axis) (B) Number 8 triangular part with a wide of 2 mm (x-axis) (C) Number 7 triangular part with a wide of 2 mm (y-axis) (D) Number 8 triangular part with a wide of 2 mm (y-axis).

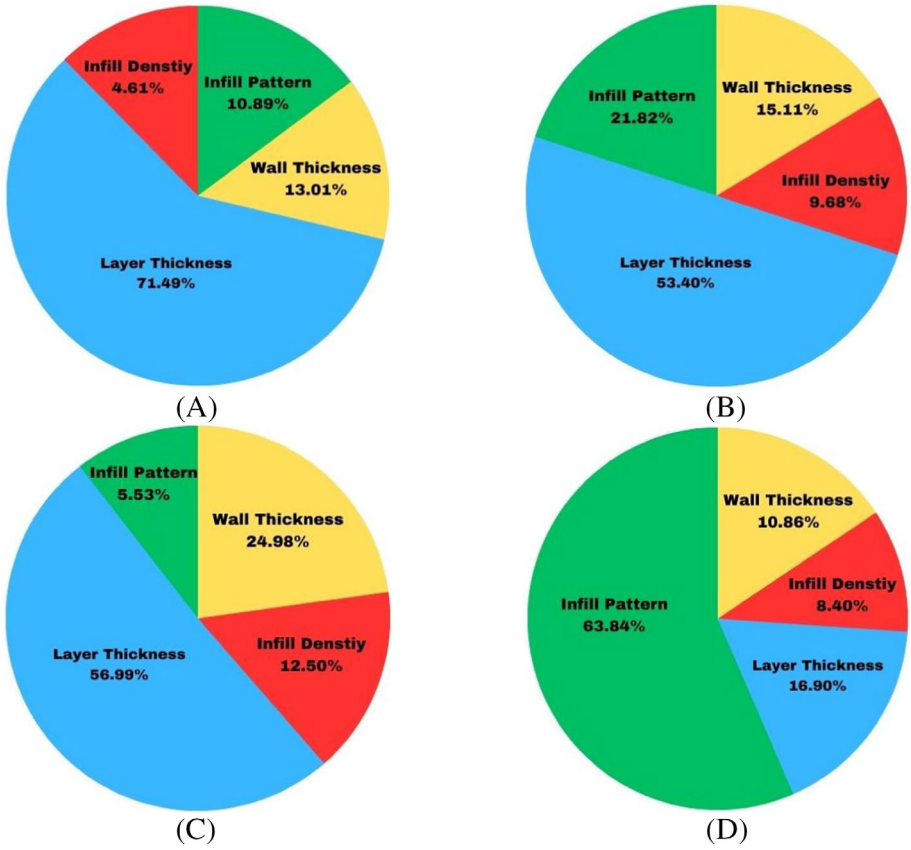

FIGURE 16 Contribution of each parameter for the x and y axes of the 4 mm wide triangular pieces. (A) Number 9 triangular part with a wide of 4 mm (x-axis) (B) Number 10 triangular part with a wide of 4 mm (x-axis) (C) Number 9 triangular part with a wide of 4 mm (y-axis) (D) Number 10 triangular part with a wide of 4 mm (y-axis).

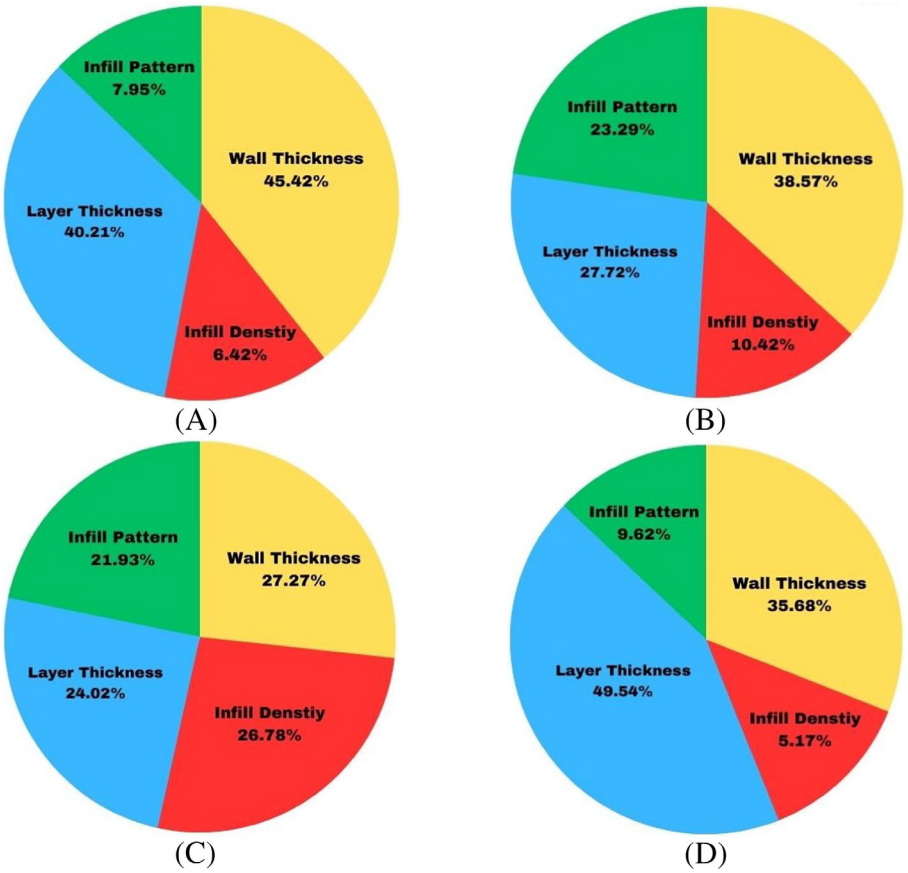

FIGURE 17 Contribution of each parameter for the x and y axes of the 2 mm wide pentagon pieces. (A) Number 11 pentagon part with a wide of 2 mm (x-axis) (B) Number 12 pentagon part with a wide of 2 mm (x-axis) (C) Number 11 pentagon part with a wide of 2 mm (y-axis) (D) Number 12 pentagon part with a wide of 2 mm (y-axis).

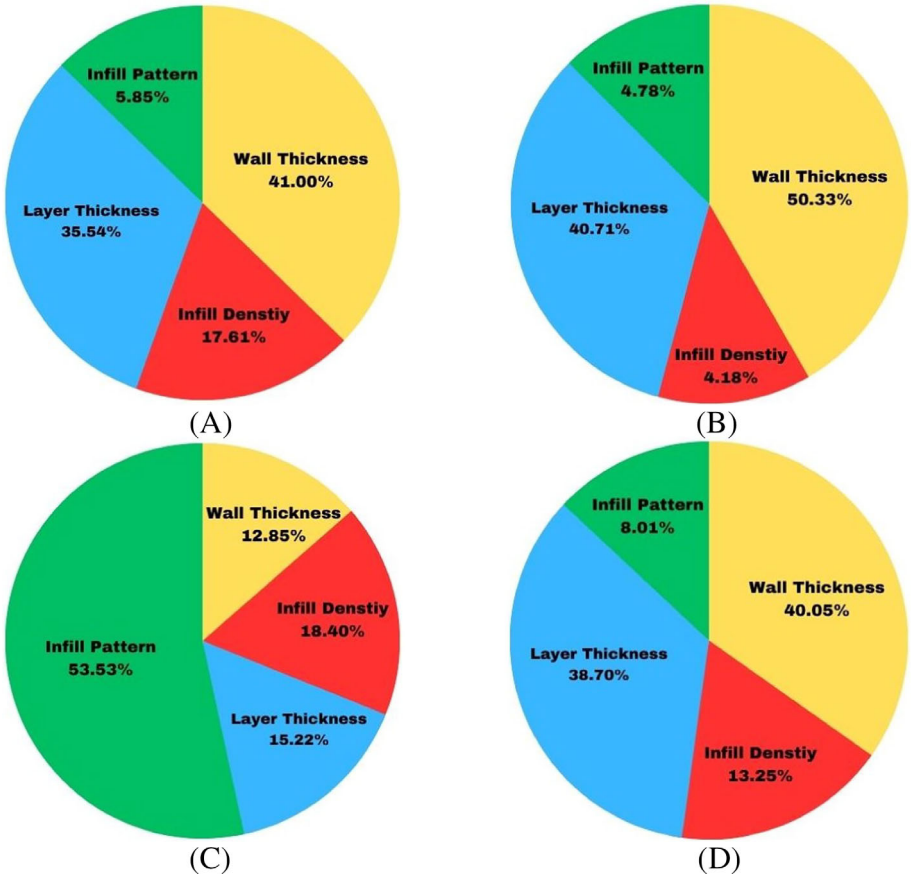

FIGURE 18 Contribution of each parameter for the x and y axes of the 4 mm wide pentagon pieces. (A) Number 13 pentagon part with a wide of 4 mm (x-axis) (B) Number 14 pentagon part with a wide of 4 mm (x-axis) (C) Number 13 pentagon part with a wide of 4 mm (y-axis) (D) Number 14 pentagon part with a wide of 4 mm (y-axis).

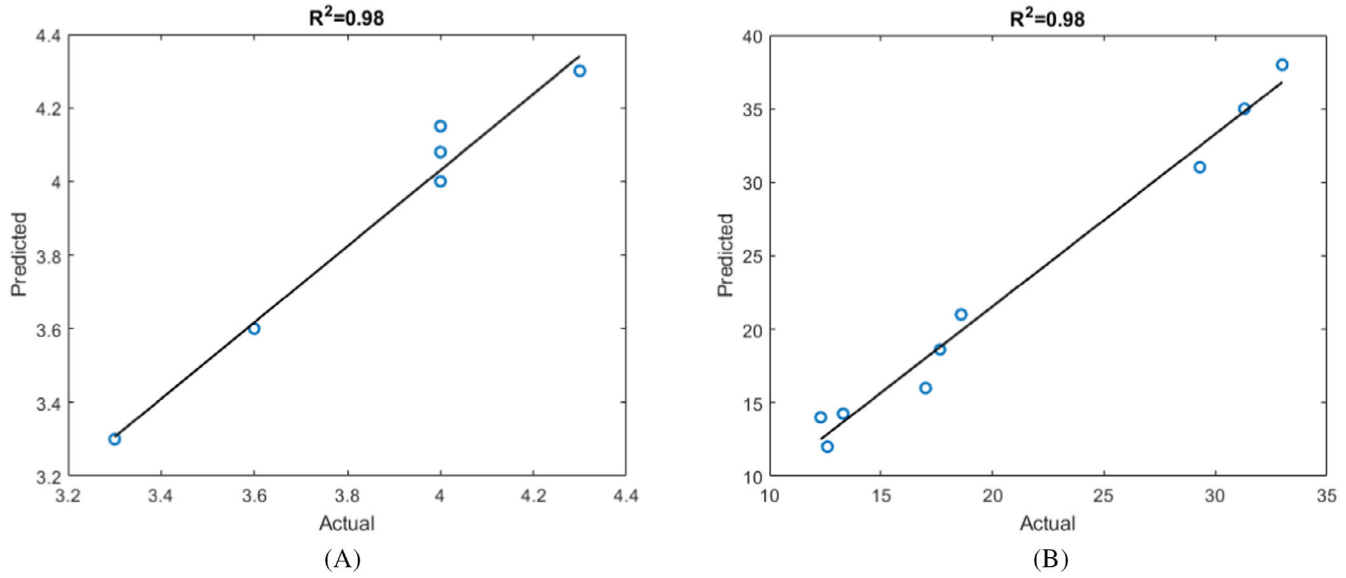

FIGURE 19 Comparison of actual and predicted values with ANN for (A) material consumption (B) printing time.

the most effective parameters in debossed cylindrical pillows with diameters of 1.5, 3, and 4.5 mm.

Figure 15 shows the contribution of printing parameters to the dimensional accuracy of 2 mm wide triangular parts in the x and y axes. The most effective parameter in the dimensional accuracy of the embossed part 7 in the x and y planes was the layer thickness (Figure 15A–C). The values of this parameter are 73.60% and 79.93% on the x and y axes, respectively. The effects of the other parameters were similar. The most effective parameters in the x and y planes of the debossed part 8 were the layer thickness and infill pattern, respectively. As a result, the contribution of the parameters affecting the dimensional accuracy of 2 mm wide triangular parts in the x and y axes was different. When Figure 15 is examined, the most effective parameter is the layer thickness.

Figure 16 shows the contribution of printing parameters to the dimensional accuracy of the 4 mm wide triangular parts in the x and y axes. The most effective parameter in the dimensional accuracy of the embossed part 9 in the x and y planes was the layer thickness (Figure 16A–C). The values of this parameter are 71.49% and 56.99% on the x and y axes, respectively. The effects of the other parameters were similar. The most effective parameters in the x and y planes of the debossed part 10 were the layer thickness and infill pattern, respectively. As a result, the contribution of the parameters affecting the dimensional accuracy of the 4 mm wide triangular parts in the x and y axes was different. When Figure 16 is examined, the most effective parameter is the layer thickness. The results are similar to the contribution rates shown in Figure 15. Changing the particle size did not significantly affect the contribution of the printing parameters.

Figure 17 shows the contribution of printing parameters to the dimensional accuracy of 2 mm wide pentagon parts in the x and y axes. The most effective parameter in the dimensional accuracy of the embossed part 11 in the x and y planes was the wall thickness (Figure 17A–C). The values of this parameter are 45.42% and 27.27% on the x and y axes, respectively. The parameter that has the lowest effect on the x and y axes is the infill pattern. The most effective parameters in the x and y planes of the debossed part 12 were the wall thickness and layer thickness, respectively. The values of these parameters are 38.57% and 49.54%, respectively. As a result, the contribution of the parameters affecting the dimensional accuracy of 2 mm wide pentagon parts in the x and y axes were different. The most effective parameter is the wall thickness (Figure 17).

Figure 18 shows the contribution of printing parameters to the dimensional accuracy of the 4 mm wide pentagon parts in the x and y-axes. The most effective parameters in the dimensional accuracy of the embossed part 13 in the x and y-planes were the wall thickness and infill pattern, respectively (Figure 18A–C). The values of these parameters are 41.00% and 53.53% on the x and y axes, respectively. The parameters with the lowest impact differ. The most effective parameter in the x and y planes of the debossed part 14 was the wall thickness. The values of this parameter are 50.33% and 40.05% in the x and y-planes, respectively. *T* the most effective parameter is the wall thickness (Figure 18). The results are similar to the contribution rates shown in Figure 17. Changing the particle size did not significantly affect the contribution of the printing parameters.

When the ANOVA results were evaluated in general, variability was observed in the printing parameters

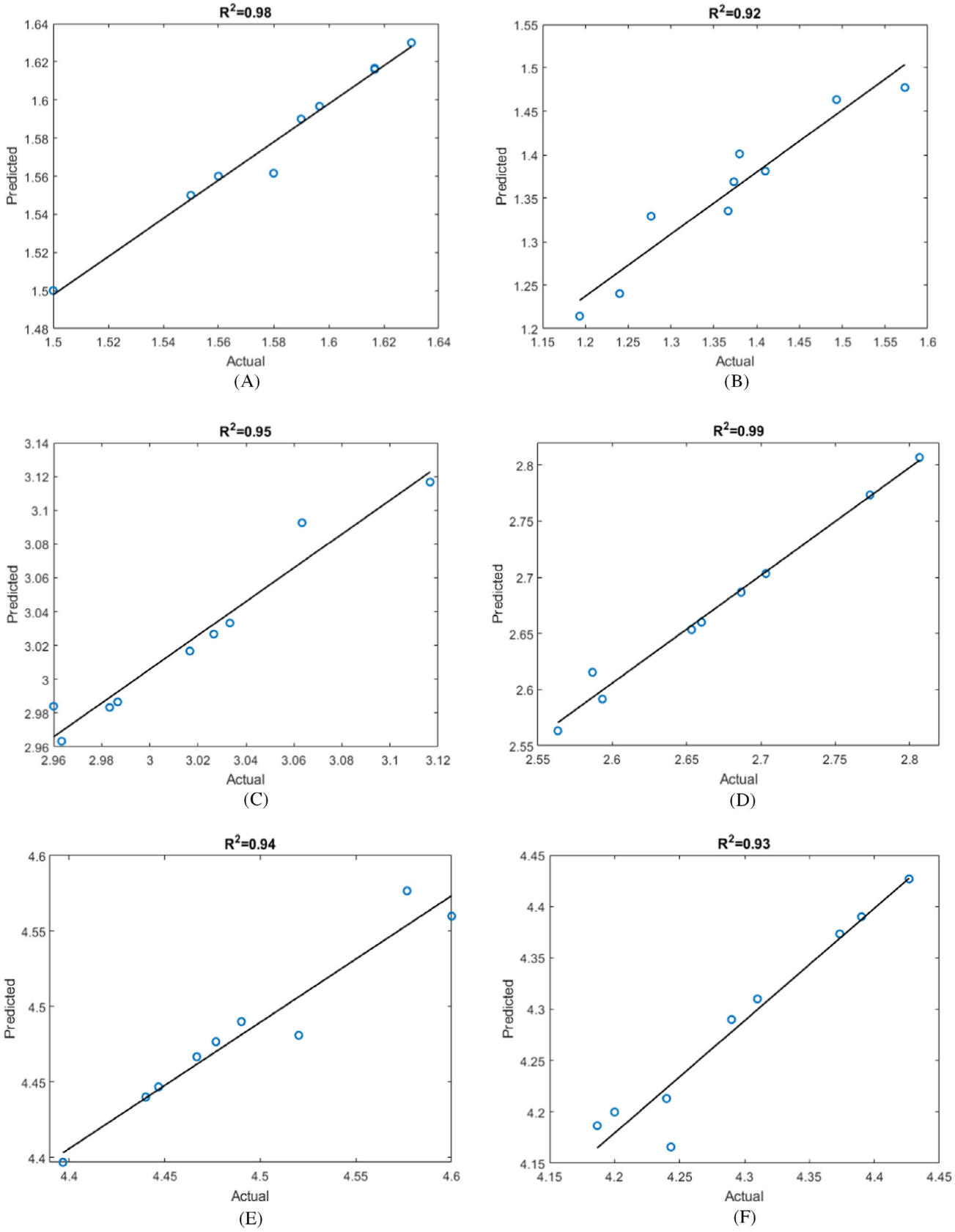

FIGURE 20 Comparison of actual and predicted diameter values with ANN for 1.5, 3, and 4.5 mm diameter cylindrical pillows. (A) Number 1 cylindrical pillow with a diameter of 1.5 mm (B) Number 4 cylindrical pocket with a diameter of 1.5 mm (C) Number 2 cylindrical pillow with a diameter of 3 mm (D) Number 5 cylindrical pocket with a diameter of 3 mm (E) Number 3 cylindrical pillow with a diameter of 4.5 mm (F) Number 6 cylindrical pocket with a diameter of 4.5 mm.

affecting the dimensional accuracy. The reason for this variability is that the temperature occurring during AM in different widths, diameters, and axes heats different parts of the parts. As each part is affected by temperature at different rates, it is assumed that different results will be observed in terms of dimensional accuracy for different widths, diameters, and axes.

3.4 | Artificial neural network results

Accurate predictions of real-time experimental outcomes in additive manufacturing (AM) technology are crucial for saving both time and cost. Therefore, it is imperative to anticipate the results of upcoming experiments in the subsequent stages and assess them accurately. Currently, numerous machine learning methods are employed for predicting the AM process.[58–60] Artificial neural networks (ANNs) find extensive use in literature for predicting the performance of manufacturing processes, with their predictive accuracy being contingent upon the quantity of experimental data available.[61] ANNs represent computer systems designed to autonomously execute tasks such as deriving new information, learning, and discovering novel insights—mimicking the human brain's characteristics without external assistance. They originated from the mathematical modeling of the learning process, drawing inspiration from the human brain's structure and its capabilities for learning, memory, and generalization.

In this study, an ANN model was employed for the numerical prediction of dimensional accuracy in AM-produced parts. The data should be shared for training,

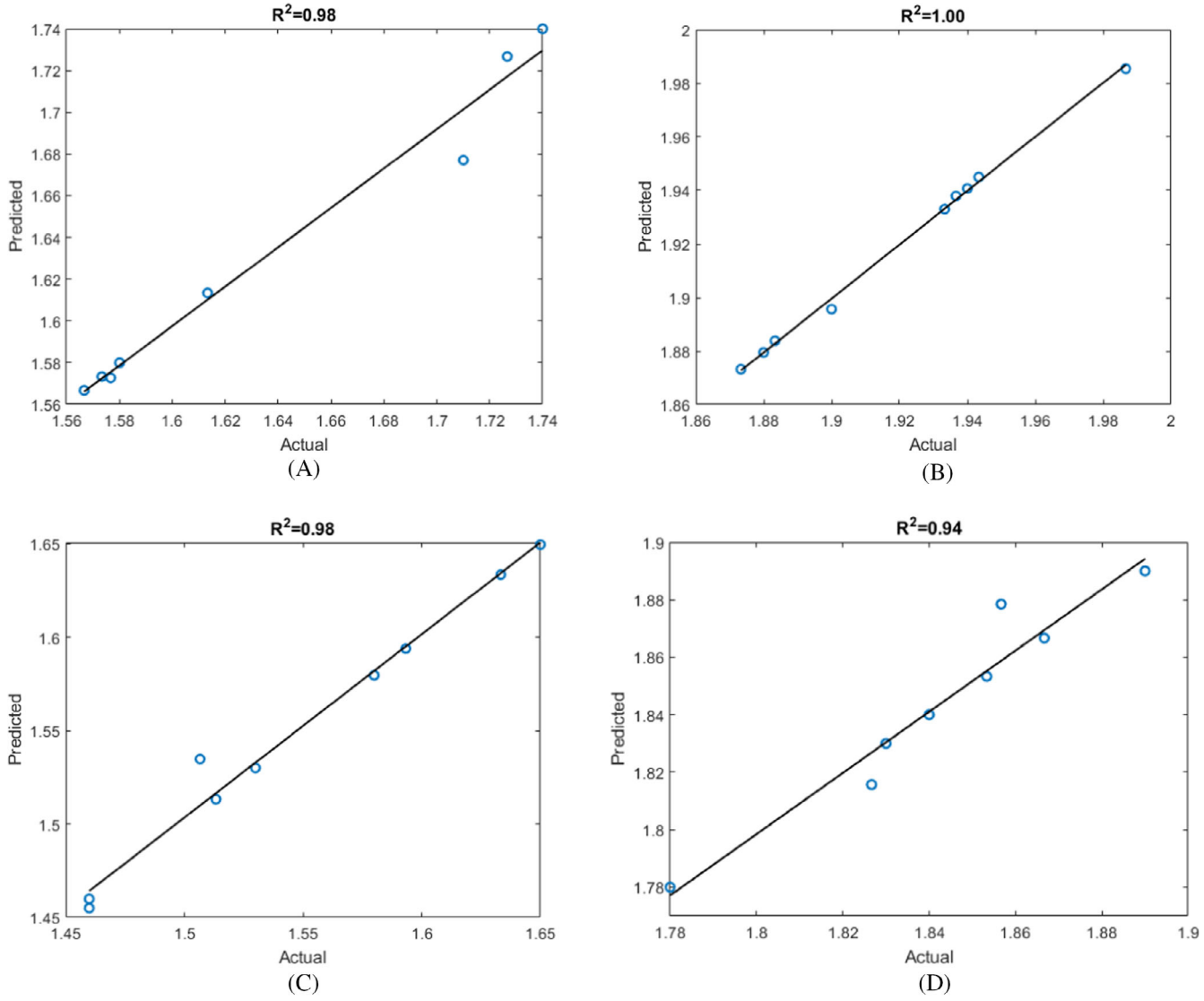

FIGURE 21 Comparison of the actual and predicted results with the ANN on the x and y axes of the 2 mm wide triangular pieces. (A) Number 7 triangular part with a wide of 2 mm (x-axis) (B) Number 8 triangular part with a wide of 2 mm (x-axis) (C) Number 7 triangular part with a wide of 2 mm (y-axis) (D) Number 8 triangular part with a wide of 2 mm (y-axis).

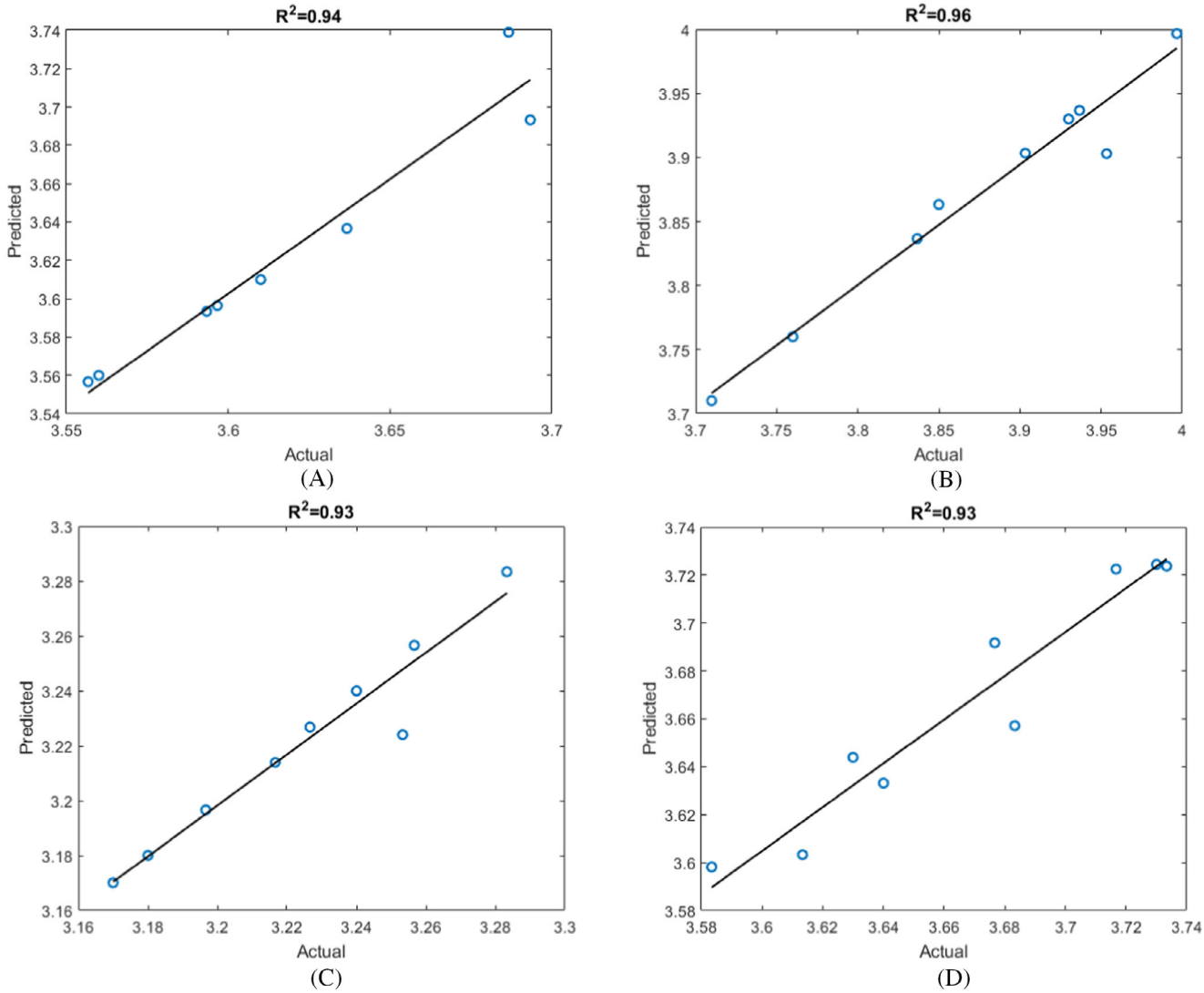

FIGURE 22 Comparison of the actual and predicted results with the ANN on the x and y axes of the 4 mm wide triangular pieces. (A) Number 9 triangular part with a wide of 4 mm (x-axis) (B) Number 10 triangular part with a wide of 4 mm (x-axis) (C) Number 9 triangular part with a wide of 4 mm (y-axis) (D) Number 10 triangular part with a wide of 4 mm (y-axis).

validation, and testing in the context of applying ANN. Therefore, a total of 198 (9 outputs × 22 combinatorial points) values are randomly employed for ANN training, validation, and testing (75% for training, 10% for validating, and 15% for testing). A feedforward neural network was selected and trained with the levenberg–marquardt algorithm in MATLAB. The preference for this algorithm stems from its ability to deliver speed and stability during ANN training.[62] One hidden layer and ten hidden neurons were used to develop model. Sigmoid activation function was used for hidden layer and output.

R-squared (R^2) criterion was used to evaluate the performance of the prediction results. This criterion is the statistical method used to evaluate the performance of the model in regression analysis. The fact that $R^2 = 1$ proves that the experimental data provide a perfectly linear curve. The ANN prediction results regarding the printing time and material consumption of the 3D printer for each experiment determined by the Taguchi method are shown in Figure 19. The prediction success for both material consumption and printing time is quite high.

First, the dimensional accuracy estimation of cylindrical pillows was performed using ANN. The results are shown in Figure 20. A comparison of actual and predicted diameter values with the ANN of 1.5 mm diameter cylindrical pillows' number 1 in Figure 20A, and number 4 in Figure 20B is given. A comparison of actual and predicted diameter values with the ANN of 3 mm diameter cylindrical pillows' number 2 in Figure 20C, and number 5 in Figure 20D is given. A comparison of actual and predicted diameter values with the ANN of 4.5 mm diameter cylindrical pillows' number 3 in Figure 20E, and number

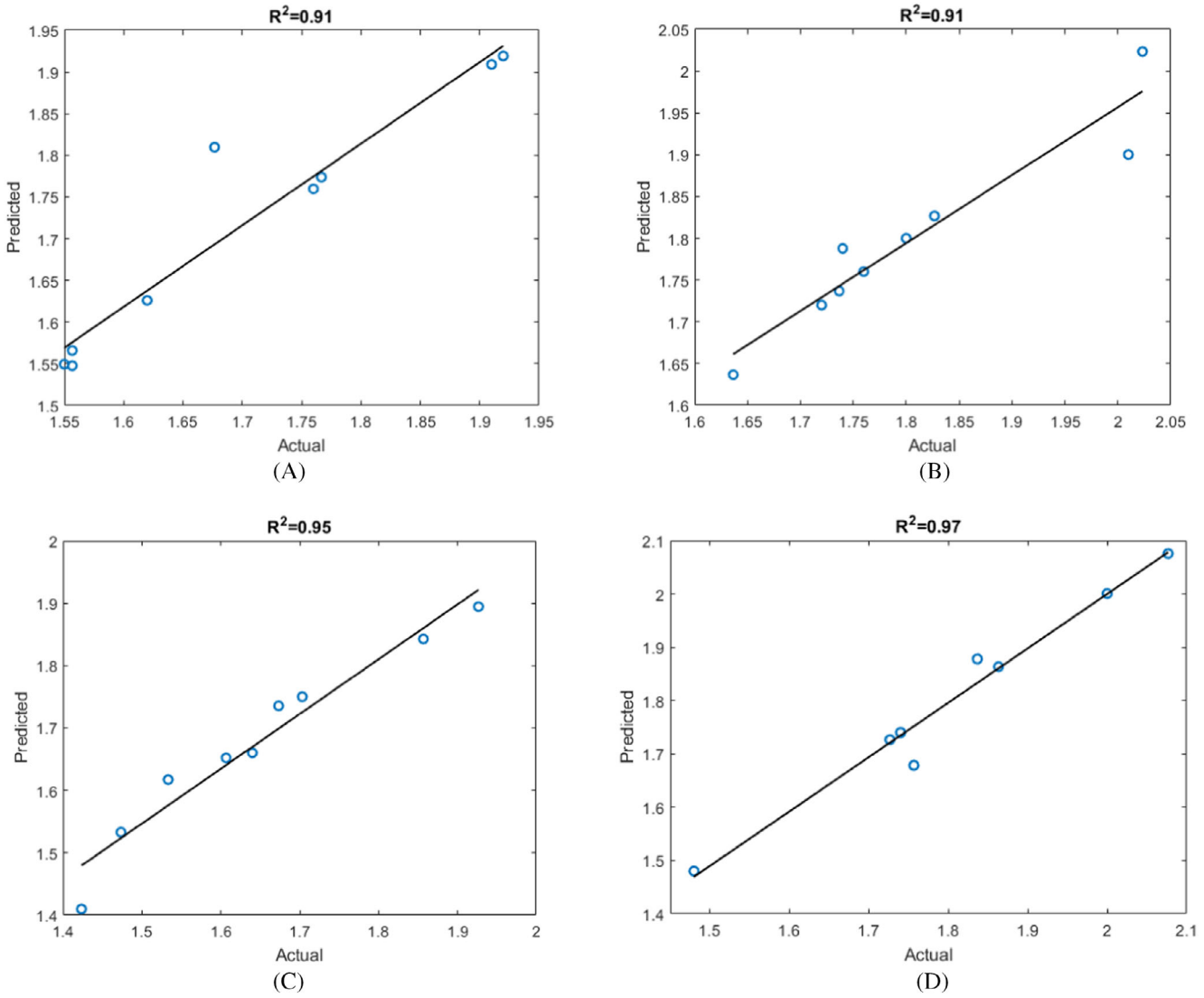

FIGURE 23 Comparison of the actual and predicted results with the ANN on the x and y axes of the 2 mm wide pentagon pieces. (A) Number 11 pentagon part with a wide of 2 mm (x-axis) (B) Number 12 pentagon part with a wide of 2 mm (x-axis) (C) Number 11 pentagon part with a wide of 2 mm (y-axis) (D) Number 12 pentagon part with a wide of 2 mm (y-axis).

6 in Figure 20F is given. The average R^2 value of a total of six cylindrical pillows was calculated as 0.95. This value shows that the prediction success is quite high. The highest success rate occurred for piece number 5.

Dimensional accuracy estimation of triangular parts after cylindrical pillows was performed using ANN. First, the widths of the 2 mm wide triangular pieces in the *x* and *y* axes were estimated (Figure 21). A comparison of the actual and predicted results with the ANN on the x-axis of the 2 mm wide triangular pieces' number 7 in Figure 21A, and number 8 in Figure 21B is shown. A comparison of the actual and predicted results with the ANN on the y-axis of the 2 mm wide triangular pieces' number 7 in Figure 21C, and number 8 in Figure 21D is shown. The prediction success rate of 2 mm wide triangular pieces is quite higher than that of cylindrical pillows.

After the ANN prediction process of 2 mm wide triangular pieces, the same method was applied to 4 mm wide triangular pieces. The dimensional accuracy estimation results in the x and y-axes of 4 mm wide triangular pieces are given in Figure 22. A comparison of the actual and predicted results with the ANN on the x-axis of the 4 mm wide triangular pieces' number 9 in Figure 22A, and number 10 in Figure 22B is shown. A comparison of the actual and predicted results with the ANN on the y-axis of the 4 mm wide triangular pieces' number 9 in Figure 22C, and number 10 in Figure 22D is shown. The success rate of 4 mm wide pieces is slightly lower than that of 2 mm wide triangular pieces. However, the average R^2 value is within the desired range.

Dimensional accuracy estimation of pentagonal parts after triangular parts was performed using ANN. First,

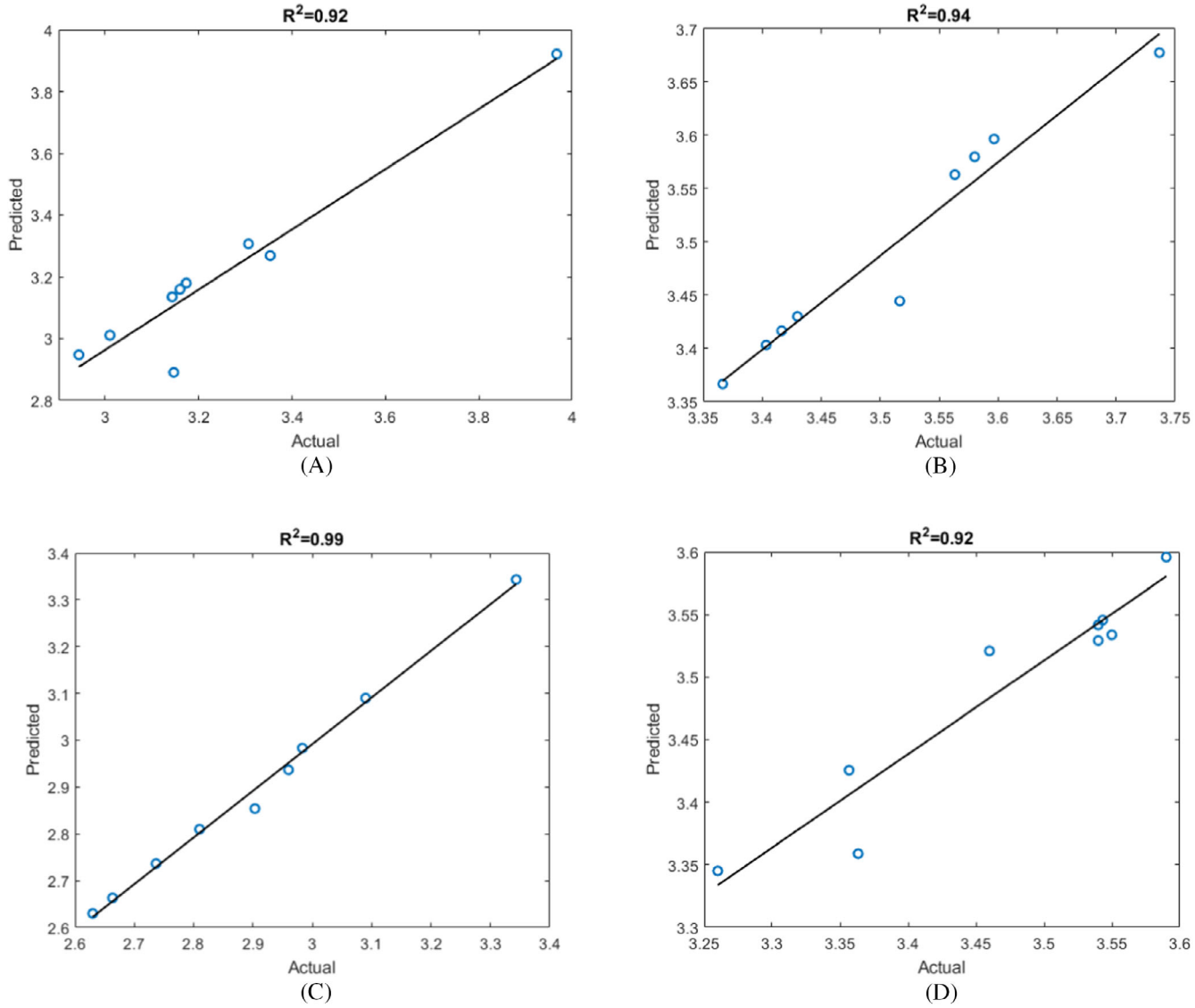

FIGURE 24 Comparison of the actual and predicted results with the ANN on the x and y axes of the 4 mm wide pentagon pieces. (A) Number 13 pentagon part with a wide of 4 mm (x-axis) (B) Number 14 pentagon part with a wide of 4 mm (x-axis) (C) Number 13 pentagon part with a wide of 4 mm (y-axis) (D) Number 14 pentagon part with a wide of 4 mm (y-axis).

the widths of 2 mm wide pentagonal pieces in the x and y axes were estimated (Figure 23). A comparison of the actual and predicted results with the ANN on the x-axis of the 2 mm wide pentagon pieces' number 11 in Figure 23A, and number 12 in Figure 23B is shown. A comparison of the actual and predicted results with the ANN on the y-axis of the 2 mm wide pentagon pieces' number 11 in Figure 23C, and number 12 in Figure 23D is shown. The average R^2 value of the ANN prediction results for 2 mm wide pentagonal pieces is 0.93.

After the ANN prediction process of 2 mm wide pentagonal pieces, the same method was applied to 4 mm wide pentagonal pieces. The dimensional accuracy estimation results in the x and y-axes of the 4 mm wide pentagonal parts are given in Figure 24. A comparison of the actual and predicted results with the ANN on the x-axis of the 4 mm wide pentagon pieces' number 13 in Figure 24A, and number 14 in Figure 24B is shown. A comparison of the actual and predicted results with the ANN on the y-axis of the 4 mm wide triangular pieces' number 13 in Figure 24C, and number 14 in Figure 24D is shown. The success rate is slightly lower than that of 2 mm wide pentagonal pieces. However, the average R^2 value is within the desired range.

4 | CONCLUSION

The main limitation of the earlier studies is that the effects of fused deposition modeling (FDM) process

parameters are analyzed on rectangular parts. This study addresses this limitation by analyzing dimensional accuracy across various geometric shapes. Specifically, the investigation centered on assessing the dimensional accuracy of basic shapes, including cylinders, triangles, and pentagons, manufactured using FDM, an additive manufacturing (AM) method. Different methodologies were employed to identify optimal printing parameters.

The experimental design process utilized the Taguchi method, incorporating four factors (infill pattern, wall thickness, infill density, and layer thickness) with three levels for each factor. A total of 27 samples were fabricated, with three samples obtained from each experiment as determined by this method. The maximum standard deviations from measurements were 0.05, indicating the repeatability of the experiments. Notably, deviations varied between debossed and embossed parts due to the size reduction of debossed parts during fabrication. The best and worst results for all pieces varied depending on the geometric shapes.

The effect of printing parameters on the dimensional accuracy of different shapes was determined with Taguchi method and ANOVA. In addition, the effect of printing parameters on material consumption and printing time was examined. The most effective parameter in material consumption was the infill density of 58.32%. Increasing this parameter increases material consumption. The effect of the layer thickness parameter on the printing time is quite high (86.28%). The effect of other parameters was approximately 5% or below. For cylindrical pillows, the best results were achieved in zigzag-concentric infill patterns, 1 mm wall thickness, 40% and 70% infill density, and 200 μm layer thickness. The most effective parameter in cylindrical pillows was the wall thickness. For the x-axis of triangular pieces, the best results were achieved in zigzag infill patterns, 2 mm wall thickness, 70% and 90% infill density, and 100 μm layer thickness. Layer thickness was the most effective parameter for x-axis triangular parts. For the y-axis of triangular pieces, the best results were achieved in zigzag-concentric infill patterns, 2–3 mm wall thickness, 40% and 70% infill density, and 100–300 μm layer thickness. The most effective parameters for the y-axis triangular parts were the infill pattern and layer thickness. For the x-axis of pentagon pieces, the best results were achieved in zigzag-concentric infill patterns, 1 mm wall thickness, 70% and 90% infill density, and 100–200 μm layer thickness. The most effective parameter for the *x*-axis pentagonal parts was wall thickness. For the *y*-axis of pentagon pieces, the best results were achieved in cubic infill patterns, 1 mm wall thickness, 40% infill density, and 100 μm layer thickness. The most effective parameters for the y-axis pentagonal parts were the infill pattern and wall thickness. These results show that it is difficult to determine the optimum printing parameter in terms of dimensional accuracy for different shapes.

Artificial neural network (ANN) was employed to assess and predict experimental outcomes, streamlining the estimation process and reducing both time and cost. To facilitate the application of ANN, the data was partitioned for training, validation, and testing, with 75% allocated for training, 10% for validation, and 15% for testing. Across all geometric shapes, the average R^2 value exceeded 95%, indicating the effectiveness of the proposed ANN model in predicting the influence of printing parameters on dimensional accuracy.

In summary, precise control of printing parameters can enhance the dimensional accuracy of 3D printed parts within the desired range. This study serves as a comprehensive guide for achieving optimal dimensional accuracy in 3D printing, encompassing various AM technologies.

ACKNOWLEDGMENTS

The authors would like to express their gratitude to Dr. M. Said BAYRAKLILAR, who generously supported the execution of this study, and also extend their thanks to the personnel of the Additive Manufacturing and Seismic Isolator Laboratory at Siirt University Faculty of Engineering for their valuable contributions.

FUNDING INFORMATION

The author received no financial support for the research, authorship, and/or publication of this article.

CONFLICT OF INTEREST STATEMENT

The author declares no conflict of interest.

DATA AVAILABILITY STATEMENT

All data underlying the results are available as part of the article and no additional source data are required.

ORCID

Osman Ulkir https://orcid.org/0000-0002-1095-0160

REFERENCES

[1] M. Touri, F. Kabirian, M. Saadati, S. Ramakrishna, M. Mozafari, *Adv. Eng. Mater.* **2019**, *21*, 21.
[2] N. K. Maurya, V. Rastogi, P. Singh, *CIRP J. Manuf. Sci. Technol.* **2020**, *29*, 53.
[3] A. Nazir, K. M. Abate, A. Kumar, J.-Y. Jeng, *Int. J. Adv. Manuf. Technol.* **2019**, *104*, 3489.
[4] O. Abdulhameed, A. Al-Ahmari, W. Ameen, S. H. Mian, *Adv. Mech. Eng.* **2019**, *11*, 168781401882288.
[5] N. Shahrubudin, T. C. Lee, R. Ramlan, *Procedia Manuf.* **2019**, *35*, 1286.
[6] J. Lee, *Processes* **2021**, *9*, 1495.

[7] N. Haghdadi, M. Laleh, M. Moyle, S. Primig, *J. Mater. Sci.* **2021**, *56*, 64.
[8] B. Ergunes, H. Gunduz, O. Ulkir, *J. Test. Eval.* **2023**, *51*, 20220605.
[9] S. Saleh Alghamdi, S. John, N. Roy Choudhury, N. K. Dutta, *Polymers* **2021**, *13*, 753.
[10] S. Yuan, F. Shen, C. K. Chua, K. Zhou, *Prog. Polym. Sci.* **2019**, *91*, 141.
[11] P. Awasthi, S. S. Banerjee, *Addit. Manuf.* **2021**, *46*, 102177.
[12] A. A. Bakır, R. Atik, S. Özerinç, *Rapid Prototyp. J.* **2021**, *27*, 537.
[13] H. J. Aida, R. Nadlene, M. T. Mastura, L. Yusriah, D. Sivakumar, R. A. Ilyas, *Int. J. Sustain. Eng.* **2021**, *14*, 1988.
[14] N. R. Madhu, H. Erfani, S. Jadoun, M. Amir, Y. Thiagarajan, N. P. S. Chauhan, *Int. J. Adv. Manuf. Technol.* **2022**, *122*, 2125.
[15] V. Mazzanti, L. Malagutti, F. Mollica, *Polymers* **2019**, *11*, 1094.
[16] S. Wickramasinghe, T. Do, P. Tran, *Polymers* **2020**, *12*, 1529.
[17] L. Suárez, M. Domínguez, *Int. J. Adv. Manuf. Technol.* **2020**, *106*, 1267.
[18] R. Nandhakumar, K. Venkatesan, *Mater. Today Commun.* **2023**, *35*, 105538.
[19] R. B. Kristiawan, F. Imaduddin, D. Ariawan, Ubaidillah, Z. Arifin, *Open Eng.* **2021**, *11*, 639.
[20] R. Patel, C. Desai, S. Kushwah, M. H. Mangrola, *Mater. Today Proc.* **2022**, *60*, 2162.
[21] M. Lalegani Dezaki, M. K. A. Mohd Ariffin, S. Hatami, *Rapid Prototyp. J.* **2021**, *27*, 562.
[22] J. Kechagias, D. Chaidas, N. Vidakis, K. Salonitis, N. M. Vaxevanidis, *Mater. Manuf. Process.* **2022**, *37*, 963.
[23] J. Retolaza, K. Gondra, R. Ansola, A. Allue, *Mater. Manuf. Process.* **2022**, *37*, 1332.
[24] A. D. Valino, J. R. C. Dizon, A. H. Espera, Q. Chen, J. Messman, R. C. Advincula, *Prog. Polym. Sci.* **2019**, *98*, 101162.
[25] A. Dey, N. Yodo, *J. Manuf. Mater. Process.* **2019**, *3*, 64.
[26] Y. Khan, A. Thielens, S. Muin, J. Ting, C. Baumbauer, A. C. Arias, *Adv. Mater.* **2020**, *32*, 32.
[27] A. Cerro, P. E. Romero, O. Yiğit, A. Bustillo, *Int. J. Adv. Manuf. Technol.* **2021**, *115*, 2465.
[28] A. W. Gebisa, H. G. Lemu, *Procedia Manuf.* **2019**, *30*, 331.
[29] J. Kechagias, D. Chaidas, *Mater. Manuf. Process.* **2023**, *38*, 933.
[30] O. Ulkir, G. Akgun, *Sci. Technol. Weld. Joining* **2023**, *28*, 548.
[31] G. D. Goh, S. L. Sing, W. Y. Yeong, *Artif. Intell. Rev.* **2021**, *54*, 63.
[32] H. D. Vora, S. Sanyal, *Prog. Addit. Manuf.* **2020**, *5*, 319.
[33] Y. Wang, Z. Xu, D. Wu, J. Bai, *Materials* **2020**, *13*, 2406.
[34] D. A. Sawant, B. M. Shinde, S. Raykar, *J. Mater. Today Proc.* **2023**.
[35] D. Jafari, T. H. J. Vaneker, I. Gibson, *Mater. Des.* **2021**, *202*, 109471.
[36] J. P. M. Pragana, R. F. V. Sampaio, I. M. F. Bragança, C. M. A. Silva, P. A. F. Martins, *Adv. Ind. Manuf. Eng.* **2021**, *2*, 100032.
[37] P. Patpatiya, K. Chaudhary, A. Shastri, S. Sharma, *Proc. Inst. Mech. Eng. Part C J. Mech. Eng. Sci.* **2022**, *236*, 7899.
[38] M. Lalegani Dezaki, A. Serjouei, A. Zolfagharian, M. Fotouhi, M. Moradi, M. K. A. Ariffin, M. Bodaghi, *Adv. Powder Mater.* **2022**, *1*, 100054.
[39] J. Jiang, *Int. J. Comput. Integr. Manuf.* **2023**, *36*, 1258.
[40] C. Wang, X. P. Tan, S. B. Tor, C. S. Lim, *Addit. Manuf.* **2020**, *36*, 101538.
[41] S. Chinchanikar, A. A. Shaikh, *J. Mater. Eng. Perform.* **2022**, *31*, 6112.
[42] S. Kumar, T. Gopi, N. Harikeerthana, M. K. Gupta, V. Gaur, G. M. Krolczyk, C. Wu, *J. Intell. Manuf.* **2023**, *34*, 21.
[43] M. G. M. Abdolrasol, S. M. S. Hussain, T. S. Ustun, M. R. Sarker, M. A. Hannan, R. Mohamed, J. A. Ali, S. Mekhilef, A. Milad, *Electronics* **2021**, *10*, 2689.
[44] K. M. Hamdia, X. Zhuang, T. Rabczuk, *Neural Comput. Appl.* **1923**, *2021*, 33.
[45] A. B. Çolak, *Int. J. Energy Res.* **2021**, *45*, 478.
[46] L. Zhu, J. Tang, Z. Luo, *AIChE J.* **2020**, *66*, 66.
[47] R. Patel, S. Jani, A. Joshi, *Int. J. Interact. Des. Manuf.* **2023**, *17*, 2115.
[48] M. Bhayana, J. Singh, B. Singh, J. Singh, *Recent Trends in Industrial and Production Engineering, Springer, Singapore* **2022**, p. 109.
[49] M. M. Hanon, L. Zsidai, Q. Ma, *Mater. Today Proc.* **2021**, *42*, 3089.
[50] O. E. Akbaş, O. Hıra, S. Z. Hervan, S. Samankan, A. Altınkaynak, *Rapid Prototyp. J.* **2019**, *26*, 288.
[51] M. S. Bayraklilar, *J. Mater. Eng. Perform.* **2023**.
[52] O. A. Mohamed, S. H. Masood, J. L. Bhowmik, *Adv. Manuf.* **2021**, *9*, 115.
[53] B. Ekinci, A. Ehrmann, *ASEC 2022*, MDPI, Basel Switzerland **2022**, p. 40.
[54] W.-H. Chen, M. Carrera Uribe, E. E. Kwon, K.-Y. A. Lin, Y.-K. Park, L. Ding, L. H. Saw, *Renew. Sustain. Energy Rev.* **2022**, *169*, 112917.
[55] M. Gavahian, R. Chu, *J. Food Process Eng.* **2022**, *45*, 45.
[56] J. D. Kechagias, *Mater. Manuf. Process.* **2023**, *9*, 1.
[57] M. Mahmoudi, S. R. Burlison, S. Moreno, M. Minary-Jolandan, *ACS Appl. Mater. Interfaces* **2021**, *13*, 5529.
[58] O. Ulkir, M. S. Bayraklılar, M. Kuncan, *Addit. Manuf.* **2023**.
[59] Z. Jin, Z. Zhang, G. X. Gu, *Adv. Intell. Syst.* **2020**, *2*, 2.
[60] Q. Zhu, Z. Liu, J. Yan, *Comput. Mech.* **2021**, *67*, 619.
[61] J. D. Kechagias, S. P. Zaoutsos, *Prog. Addit. Manuf.* **2023**.
[62] F. Yildirim Dalkiran, M. Toraman, *Aircr. Eng. Aerosp. Technol.* **2021**, *93*, 35.

How to cite this article: S. Gunes, O. Ulkir, M. Kuncan, *J. Polym. Sci.* **2024**, *62*(9), 1864. https://doi.org/10.1002/pol.20230876